

# SANet: A Semantic-aware Agentic AI Networking Framework for Cross-layer Optimization in 6G

Yong Xiao, *Senior Member, IEEE*, Xubo Li, Haoran Zhou, Yingyu Li, Yayu Gao, Guangming Shi, *Fellow, IEEE*, Ping Zhang, *Fellow, IEEE*, and Marwan Krunz, *Fellow, IEEE*



**Abstract**—Agentic AI networking (AgentNet) is a novel AI-native networking paradigm in which a large number of specialized AI agents collaborate to perform autonomous decision-making, dynamic environmental adaptation, and complex missions. AgentNet has the potential to facilitate real-time network management and optimization functions, including self-configuration, self-optimization, and self-adaptation across diverse and complex environments, laying the foundation for fully autonomous networking systems in the future. Despite its promise, AgentNet is still in the early stage of development, and there still lacks an effective networking framework to support automatic goal discovery and multi-agent self-orchestration and task assignment. This paper proposes SANet, a novel semantic-aware AgentNet architecture for wireless networks that can infer the semantic goal of the user and automatically assign agents associated with different layers of the network to fulfill the inferred goal. Motivated by the fact that AgentNet is a decentralized framework in which collaborating agents may generally have different and even conflicting objectives, we formulate the decentralized optimization of SANet as a multi-agent multi-objective problem, and focus on finding the Pareto-optimal solution for agents with distinct and potentially conflicting objectives. We propose three novel metrics for evaluating SANet: (the agents' objective) optimization error, (dynamic environment) generalization error, and (multi-objective) conflicting error. Furthermore, we develop a model partition and sharing (MoPS) framework in which large models, e.g., deep learning models, of different agents can be partitioned into shared and agent-specific parts that are jointly constructed and deployed according to agents' local computational resources. Two decentralized optimization algorithms, static-weighting and dynamic-weighting algorithms, are introduced to

*\*This work is submitted to IEEE for possible publication. Copyright may be transferred without notice, after which this version may no longer be accessible. An earlier version of this paper will be presented in part at the Proceedings of the IEEE GLOBECOM, Taipei, Taiwan, December 2025 [1].*

Yong Xiao, Xubo Li, Haoran Zhou, and Yayu Gao are with the School of Electronic Information and Communications, the Huazhong University of Science and Technology, Wuhan, China 430074. Yong Xiao is also with the Peng Cheng Laboratory, Shenzhen, China, and Pazhou Laboratory (Huangpu), Guangzhou, China (e-mail: yongxiao@hust.edu.cn).

Y. Li is with the School of Mechanical Engineering and Electronic Information, China University of Geosciences (Wuhan), China, 430074 (e-mail: liyingyu29@cug.edu.cn).

G. Shi is with the Peng Cheng Laboratory, Shenzhen, China 518055, also with the School of Artificial Intelligence, Xidian University, Xi'an, Shaanxi 710071, China (e-mail: gmshi@xidian.edu.cn). (e-mail: gmshi@xidian.edu.cn).

P. Zhang is with the State Key Laboratory of Networking and Switching Technology, Beijing University of Posts and Telecommunications, Beijing, China 100876 (email: pzhang@bupt.edu.cn).

M. Krunz is with the Department of Electrical and Computer Engineering, the University of Arizona, Tucson, AZ 85721 (e-mail: krunz@arizona.edu).

optimize the above three metrics. We derive theoretical bounds for all these performance metrics and prove that there exists a three-way tradeoff among optimization, generalization, and conflicting errors. Finally, to validate our theoretical results, we develop an open-source Radio Access Network (RAN) and core network-based hardware prototype that implements three Transformer-based time-series prediction agents to interact with three different layers of the network. Experimental results show that the proposed MoPS framework achieved performance gains of up to 14.61% while requiring only 44.37% of the Floating-Point Operations (FLOPs) for inference at each agent compared to state-of-the-art algorithms. Also, compared to the static-weighting algorithm, the dynamic-weighting algorithm achieves up to 83.81% reduction in training errors caused by conflicting objectives.

**Index Terms**—Agentic AI networking, AI agent, semantic-aware network, 6G.

## 1 INTRODUCTION

Wireless network systems have long utilized a centralized and layered architecture, primarily due to its inherent structural simplicity and ease of management. The fast-growing demand for emerging applications and services, such as immersive mixed reality (XR)-based immersive communication [2], semantic communication [3], [4], and ambient intelligence [5], most of which require high computation and communication loads to be processed efficiently at the network edge, has recently rendered the existing architecture a major performance and scalability bottleneck. Specifically, the existing layered design requires that any tactical decision made at the edge must be monitored and approved by higher-layer entities, which causes intolerably high communication overhead and latency. Furthermore, the recent trend toward deep integration of Artificial Intelligence (AI) and communication networking has further exacerbated these challenges, as the architecture must now support a large volume of data that needs to be constantly generated, transferred, and processed across layers. Recent works focused on the cross-layer optimization, particularly those leveraging distributed optimization techniques, have proposed useful theoretical solutions to mitigate these issues; however, they often require pre-defined and carefully designed multi-layer decomposition schemes and coordinated objectives with limited flexibility and scalability.

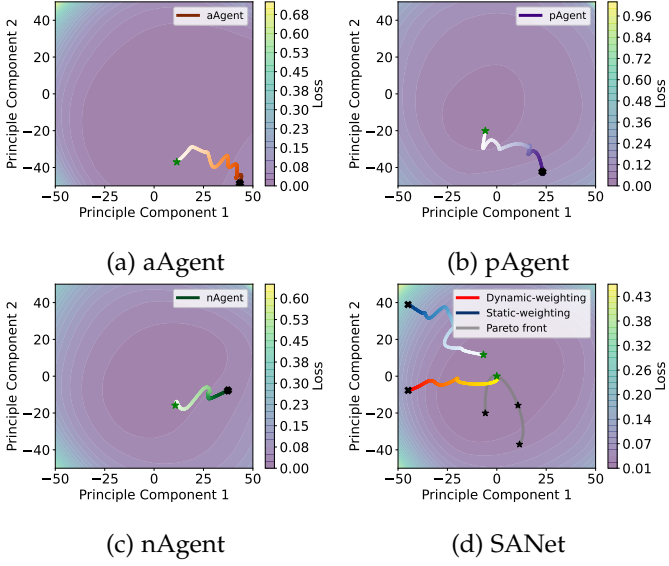


Fig. 1: (a)-(c) Learning trajectories of three agents deployed at the physical layer (pAgent), application layer (aAgent), and network layer (nAgent) of a wireless network (black  $\star$  denotes the initialization of the model, green  $\star$  denotes the end point); (d) SANet's collaborative learning trajectories of all three agents using static- and dynamic-weighting algorithms where grey line denotes the Pareto front, black  $\star$  denotes the local optimum of each agent.

This has led to the emergence of the agentic AI networking (*AgentNet*), a flexible, goal-driven networking framework that focuses on the autonomous interaction and self-adaptation of a diverse group of AI agents for different goals. Unlike existing AI-based network optimization solutions that are primarily built on a closed-loop and passive learning framework and learned solely from a fixed training dataset, agents in *AgentNet* can actively seek new information, explore possibilities, and leverage real-world knowledge and experience to achieve a wide range of goals, thereby minimizing the influence of potential bias within the initial training dataset [6]–[9].

Despite its promise, *AgentNet* is still in the early stage of development [10]. In particular, due to its decentralized nature, coordinating and jointly optimizing the actions, goals, and objectives of different agents becomes notoriously challenging, often leading to new issues such as suboptimal consensus mechanisms, difficulties in network-wide performance benchmarking, and risks in compromising the security and trust of *AgentNet*. To shed more light on the challenges of decentralized optimization of different agents, we consider an *AgentNet* consisting of three different agents deployed in the application layer (aAgent), physical layer (pAgent), and network layer (nAgent), with different objective functions for predicting user's semantic demands, CSIs of wireless channels, and network layer traffics. We present in Fig. 1(a)-(c) the learning trajectories as well as the contours of the objective functions of these three agents. We can observe that different objective functions of agents generally result in different learning trajectories. When all three agents are selected to collaborate in optimizing their model performance and generalization performance, if no extra conflict-resolving mechanisms are enforced, e.g., the

static-weighting algorithm in Fig. 1(d), most agents may get stuck in some initializations, instead of converging to the Pareto front (the set of values in the objective space that includes all Pareto optimal solutions). By employing the conflict-resolving mechanism as developed in our proposed dynamic-weighting algorithm, the learning trajectories of agents can navigate through these conflicting objectives and converge to the Pareto front.

So far, most research efforts have focused on multi-agent task planning and adaptation, ignoring the fact that the networking architecture plays a fundamental role in the effectiveness of *AgentNet* systems. In particular, a recent study has already suggested that *AgentNet* is in essence a new communication networking paradigm that focuses on the effective communication and seamless interaction between users and agents, as well as among diverse agents within a networked system [6]. This is fundamentally different from the existing disjoint computation-communication architecture in which AI model-based modules are deployed as plugins or over-the-top applications to enhance the data transportation and delivery capabilities of a networking system. There is still a lack of a comprehensive framework that can automatically detect a user's semantic goal and self-orchestrate and coordinate the communication networking functions and model development of agents in a decentralized fashion to fulfill the identified goal.

In this paper, we propose a semantic-aware *AgentNet* framework, called SANet, for cross-layer optimization. According to SANet, the user's semantic demand can be automatically detected, and the agent controller can directly select a set of agents deployed across multiple layers of a wireless system to collaboratively deploy models that address the sensed demand. In particular, the agent controller does not know the datasets, states, and final decisions of the agents, but can convert the recognized goal into a set of subtasks to be distributed to the agents. Each agent corresponds to a physical or logical entity composed of a single model or a set of models and action functions designed with certain objectives to meet a specific goal. Different agents can have different computational capabilities and are tailored to optimize different objectives, depending on their engagement with heterogeneous datasets and data modalities. This is fundamentally different from existing cross-layer optimization solutions, which require a manually crafted multilayer task separation and coordination scheme, as well as a carefully tailored objective for each separated task that aligns with the unique characteristics and goals of each specific layer.

SANet represents a paradigm shift from the traditional data delivery-focused to the semantic goal-driven and solution-finding-focused networking. The performance metrics for evaluating SANet will therefore no longer be the same as those traditional data delivery metrics, e.g., data rate or packet delivery error. New agenticness-relevant metrics, such as the agents' optimization performance and model generalization performance, would be introduced to access SANet. In addition, since SANet is a decentralized framework in which different agents pursue distinct, often conflicting, objectives, it is generally impossible to find a globally optimized solution that maximizes the performance of all agents. Accordingly, in this paper, we focus on finding

the Pareto-optimal solution that targets the best possible trade-offs among agents of conflicting objectives.

We propose a multi-agent collaborative learning framework, called MoPS, for SANet that employs model sharing and partitioning, where large models (e.g., deep learning models) for different agents' objectives are partitioned into shared and agent-specific parts that are jointly constructed and deployed according to agents' local computational resources. We consider three novel metrics for evaluating the SANet's performance: the agents' objective optimization error, dynamic-environment generalization error, and multi-objective conflicting error. Two decentralized optimization algorithms, static-weighting and dynamic-weighting, are introduced to optimize these three metrics. We derive theoretical bounds for all three metrics and prove that there exists a three-way tradeoff among optimization, generalization, and conflicting errors. Finally, we experimentally validate SANet by developing an open-source Radio Access Network (RAN) and core network-based hardware prototype, in which we deploy agents associated with three different layers. Our results show that the proposed MoPS provides up to 14.61% performance gains with only 44.37% of the Floating-Point Operations (FLOPs) required for inference at each agent compared to state-of-the-art algorithms. Our proposed dynamic-weighting algorithm reduces up to 83.81% training errors caused by conflicting objectives, compared to the static-weighting algorithm.

The main contributions of the paper are as follows:

**(1) AgentNet-based framework for cross-layer optimization:** We introduce a general framework for cross-layer optimization in wireless networks. In this framework, an agent controller can proactively identify the user's semantic goal and divide this goal into multiple subtasks associated with agents deployed at three different layers of a wireless system (application layer, network layer, and physical layer). Different agents interact with different environments and have different local datasets and optimization objectives. We formulate the decentralized optimization of SANet as a multi-agent multi-objective problem and focus on finding the Pareto-optimal solution among agents with distinct and potentially conflicting objectives. We propose three novel metrics for evaluating the SANet's performance.

**(2) Multi-agent model sharing and partitioning:** We propose a multi-agent collaborative learning framework, MoPS, based on model sharing and partitioning in which multiple large models, e.g., deep learning models, deployed at different agents for different subtasks can be partitioned into a shared-part and agent-specific parts. The two parts are jointly constructed using two new unified interfaces: the embedding coordination interface (E-interface) and the gradient coordination interface (G-interface). We propose two decentralized optimization algorithms: static and dynamic-weighting, to jointly optimize the agents' optimization, generalization, and conflicting errors under different communication and computational resource costs.

**(3) Theoretical analysis of the three-way tradeoff:** We derive bounds on the optimization, generalization, and conflicting errors under the static and dynamic-weighting algorithms. Based on these bounds, we provide a theoretical characterization of the three-way tradeoff among optimization, generalization, and conflicting error of SANet.

**(4) Prototype and experiments:** We develop a hardware/software platform, consisting of an open-source RAN and softwareized 5G core network, and deploy three types of agents at the application, network, and physical layers in this platform to evaluate the SANet performance. Experiment results show that the proposed MoPS provides up to 14.61% performance gains with only 44.37% of the Floating-Point Operations (FLOPs) required for inference at each agent compared to state-of-the-art algorithms. Our proposed dynamic-weighting algorithm reduces up to 83.81% training errors caused by conflicting objectives, compared to the static-weighting algorithm.

## 2 RELATED WORK

### 2.1 Cross-layer Optimization

Recent results have already demonstrated that joint optimization of multiple layers in a wireless system has the potential to mitigate the inherent limitations of traditional layered networking architectures and to significantly improve resource utilization, thereby meeting the increasingly stringent QoS demands of emerging applications. Existing work often focuses on multi-layer joint optimization of a specific part of a networking system, e.g., the RAN or the transmission networks of terrestrial communication systems or satellite networks. For example, the authors in [11] showed that the spectrum efficiency of the C-RAN can be improved by jointly optimizing the parameters across the physical, data link, and transport layers, while guaranteeing the statistical end-to-end QoS. The authors in [12] proposed a mixed discrete-and-continuous variable combinatorial solution to jointly optimize user scheduling at the MAC layer and beamforming at the physical layer in a multiuser multi-antenna system. Numerical results showed that their solution significantly increases the sum rate, while maintaining the per-user QoS level and the maximum allowable transmit power of the system. Progress has also been made in specialized wireless systems, such as Reconfigurable Intelligent Surface (RIS)-assisted wireless systems and satellite networks. In particular, in [13], the authors proposed a deep reinforcement learning approach to jointly optimize the application layer video quality and the physical layer environment controlled by RIS [13]. The authors in [14] investigated the cross-layer topology optimization of a hybrid network, consisting of both Very Low Earth Orbit (VLEO) observation satellites and LEO communication satellites. A distributed multi-objective cross-layer topology optimization algorithm was proposed to jointly optimize the transmission requirements of observation satellites, load balancing among the communication satellite layer, and the transmission delay of emergency tasks.

Existing solutions often require a predefined and carefully designed multi-layer decomposition scheme. The objectives must be manually crafted to fit the specific characteristics and goals of each layer. In this paper, we focus on autonomous and decentralized cross-layer optimization based on AgentNet, in which an agent controller can proactively sense the semantic goals of users and autonomously divide the sensed goal into different subtasks to be addressed by agents at different layers. Our proposed framework is general and can preserve the layered architecture

of existing systems while facilitating scalable, adaptive, and cooperative decision-making that can better accommodate dynamic network conditions and heterogeneous requirements.

## 2.2 AI-based Network Optimization

AI-based models and solutions have been increasingly deployed to optimize various parts of the networking architecture, from smart applications and services to RAN as well as the core networks [15], [16]. Compared to traditional optimization-based solutions that rely on simplified, static models, AI-based solutions leverage data-driven learning, which can efficiently solve computationally intractable, high-dimensional, and non-convex optimization problems presented by the scale and heterogeneity of modern wireless systems. For example, various AI-based solutions have already been adopted for analysis, estimation, and optimization of physical layer environments. In particular, the authors in [17] proposed a novel zero-shot physical layer model transfer framework, SANSee, which employs a physical layer semantic-aware network (pSAN) to characterize data correlations across different physical locations. A zero-shot transfer learning-based solution was introduced to allow location-specific models to be directly transferred from a limited number of pre-trained models, achieving accuracy comparable to locally trained, supervised models. The authors in [18] applied Deep Reinforcement Learning (DRL) to solve the NP-Hard problems of channel assignment and access point clustering within distributed multi-user MIMO (D-MIMO) Wi-Fi networks. Numerical results showed that the proposed DRL framework allows an agent to learn optimal policies for maximizing user throughput and fairness, achieving a 20% performance gain compared to conventional heuristics. AI-based solutions were also applied to optimize the end-to-end data latency and reliability of a mobile networking system. In particular, the authors in [19] applied a multi-agent deep reinforcement learning (DRL)-based joint resource allocation approach to minimize the long-term delay in a cellular-based mobile edge computing (MEC) system. Experimental results demonstrated substantial improvement of over 176% in uplink transmission rate and reduction in the long-term average delay compared to conventional non-AI-based MEC systems. AI-based network optimization also attracted significant interest from the industry. Recently, the AI-RAN Alliance was established to accelerate the integration of AI into RAN technologies to improve the spectrum utilization and energy efficiency [20]. AI capabilities and functions were also incorporated into the core network architecture since the very first version of 5G. More specifically, the Network Data Analytics Function (NWDAF) was introduced as a key functional component for data analysis and processing in 3GPP Release 15 [21]. Its scope and capability were extended significantly since that release. For example, Release 18 has emphasized the integration of AI and ML into NWDAF, enabling more sophisticated analytics and automation capabilities [22]. NWDAF in Release 19 focuses on providing the necessary insights and recommendations for supporting self-optimization and self-healing [23]. ITU-T and IMT-2030 (6G) promotional group have also initiated the work for standardizing the

semantic-aware networking for future networks with the main objective to enable the networking systems to learn and adapt according to the dynamics of users' semantics and network intents [24], [25].

Despite considerable research progress in this domain, the majority of AI-based network optimization solutions employ passive learning frameworks that are trained exclusively on historical datasets. These methods operate under the often-invalid premise that past statistical data patterns will persist across future deployments, thereby limiting their capacity to adapt effectively to the increasingly dynamic, diversified, and personalized service requirements of modern telecommunication environments [26]. In this paper, we propose an AgentNet-based solution in which the user's semantic goal and demand can be predicted and proactively addressed by a carefully selected subset of collaborative agents.

## 2.3 Agentic AI and AgentNet

Agentic AI systems have attracted significant interest recently due to their potential to fundamentally shift the paradigm from reactive, passive, and monolithic learning-based models to autonomous, goal-driven, multi-agent cooperation architectures based on decentralized learning and solution finding. Critically, these systems are evolving towards a decentralized structure where heterogeneous AI agents, each with distinct skillsets, specialized knowledge, and optimization objectives, collaborate directly on peer-to-peer networks to achieve a complex, shared goal. This approach offers significant advantages over traditional centralized systems, which suffer from single points of failure, scalability bottlenecks, and high latency. Furthermore, the decentralized learning framework differs from most existing distributed learning systems (such as Federated Learning) by enabling autonomous decision-making and real-time interaction during execution, rather than solely focusing on the distributed implementation of a single centralized goal. The resulting system is inherently more resilient and fault-tolerant, as the failure of one AI agent does not compromise the operation of the entire system, and it promotes enhanced privacy by keeping sensitive data local to each agent [27]. Most existing research focuses on exploring the reasoning capacities for multi-agent planning, tool use, memory, and perception of dynamic environments to enable complex, multi-step execution [28]. Significant milestones include the development of multi-agent systems (MAS) and orchestration frameworks that facilitate cooperation and communication between specialized agents to decompose and solve high-level tasks, yielding measurable improvements in efficiency across diverse domains. For example, the authors in [29] focus on optimized task decomposition and resource allocation among agents for maximizing parallel efficiency and minimizing communication overhead. A key direction in this research involves defining explicit, communicative roles for LLM agents, as demonstrated by the work in [30]. In this work, the authors proposed the CAMEL framework, where agents are prompted into a cooperative role-playing dynamic to solve complex tasks through guided conversation. Furthermore, the capability for complex and long-horizon planning has been explored through emergent behaviors in large-scale social simulations [31], where agents

like the Generative Agents demonstrate sophisticated memory, planning, and persistent identity. To ensure reliable execution in dynamic and uncertain environments, recent work has specifically addressed robustness in multi-step planning and tool use, often by incorporating dynamic feedback mechanisms and self-correction modules [32]. Also, the authors in [33] explored the principle of iterative refinement, where agents assess and refine their own or peers' outputs using a chain-structure-based self-critique. Building on the collective strength of diverse models, the recently proposed Mixture-of-Agents (MoA) methodology introduces a layered aggregation architecture [34]. This drive toward structured intelligence is further evidenced by approaches focused on hierarchical planning and emergent control structures within agent teams [35]. In MoA, multiple LLM agents iteratively process and synthesize candidate responses from previous layers to produce a final, high-quality output, achieving state-of-the-art results on several reasoning and alignment benchmarks. Furthermore, novel performance metrics for multi-agent collaborations were introduced to focus on the length and complexity of tasks they can autonomously complete, demonstrating an exponential increase in capability [27].

AgentNet is an agentic AI-native networking system that is composed of diverse AI agents with autonomy, goal-oriented behavior, and adaptability, enabling them to make independent decisions and execute actions to achieve specific objectives with no or minimal human supervision [36]. In our previous work [6], we introduced a Generative Foundation Model (GFM)-based architecture that facilitates interaction, collaborative learning, and efficient knowledge transfer among multiple GFM-as-agents. Key performance metrics for measuring the performance of AgentNet were introduced, including implementable environment complexity, model generalization, multi-domain knowledge-based reasoning capability, resource requirements, and complex goal achievability. Two 6G applications, digital-twin industrial automation and metaverse-based infotainment systems, were considered to describe how AgentNet can be designed to support efficient task-driven interactive networking systems with diverse AI agents.

Agentic AI systems and AgentNet are still in the early stages of development. In this work, we take steps to develop novel solution concepts and performance metrics of the general AgentNet system. More specifically, motivated by the fact that AgentNet is a decentralized system, we consider the Pareto optimal solution, instead of the global optimal solution, to characterize the tradeoff among different performance metrics. We investigate the three-way tradeoff among optimization, generalization, and conflict-resolving performance of AgentNet from both theoretical and practical perspectives. To the best of our knowledge, this is the first work that investigates the AgentNet for cross-layer optimization of a wireless networking system.

### 3 SYSTEM MODEL AND PROBLEM FORMULATION

#### 3.1 System Model

We consider a general AgentNet-based cross-layer optimization problem for a wireless networking system, as illustrated in Fig. 2(a).

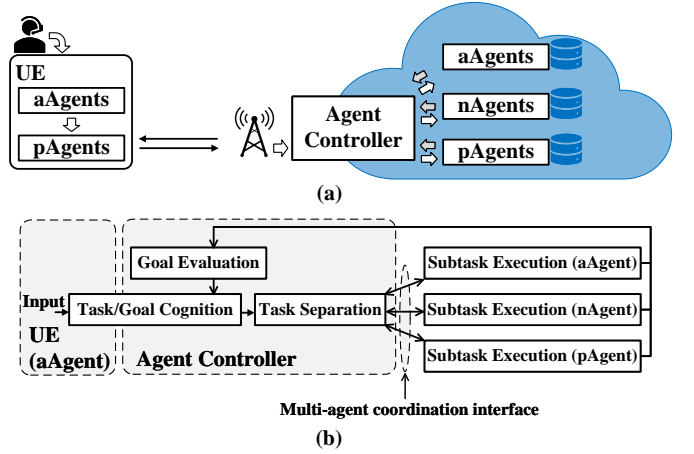


Fig. 2: (a) System model, and (b) operational workflow for a general AgentNet-based cross-layer optimization framework for wireless networks.

We consider a finite task space and let  $\mathcal{M}$  be the set of tasks that can be performed by a set of agents. To simplify our description, in this paper, we focus on coordination and collaborative learning involving at most three different types of agents deployed in three different layers: application layer, network layer, and physical layer, labeled with superscripts  $a$ ,  $n$ ,  $p$ , respectively. Our proposed solution, however, can be directly extended to more complex systems that include agents in more layers, as will be illustrated later.

(1) *Application layer agent (aAgent)*: This corresponds to the agent that can directly interact with users through some application interfaces and can adjust a range of application parameters according to the semantics of the users. For example, live streaming applications such as video conferencing and metaverse-based interactive gaming installed on smart devices can infer and predict the semantic request of the users based on the input of the application interface and adjust the application parameters, such as video resolutions and refresh rates, according to the predicted request. More formally, we define an aAgent by a tuple  $\mathcal{G}^a = \langle \mathcal{A}^a, \mathcal{S}^a, \Gamma^a, \mathcal{D}^a \rangle$  where  $\mathcal{A}^a$  is the set of acts that can be taken by aAgent,  $\mathcal{S}^a$  is the set of environmental states for an aAgent to sense and decide its act,  $\Gamma^a$  is the set of task-specific loss functions for aAgent to optimize, and  $\mathcal{D}^a$  is the set of data samples for training the aAgent's model. In this paper, we consider a specific AgentNet system in which each agent consists of an AI model and an action function. In particular, an AI model with parameters  $\omega^a$  can be trained to proactively sense and predict the future semantic goal of users based on the currently observed state and the observation history, and an act function will decide the specific action to be taken based on the model output. Generally speaking, the aAgent cannot control the decision-making processes of other agents. Its performance, however, can be influenced by the actions of other agents, including those in the physical layer and network layer. We can write the loss function of aAgent when being selected to address task  $m$  as  $\mathcal{L}_m^a(\Omega_m, \mathcal{D}^a) = \frac{1}{|\mathcal{D}^a|} \sum_{d^a \in \mathcal{D}^a} \ell_m^a(\Omega_m, d^a)$  where  $\ell_m^a \in \Gamma^a$ ,  $\Omega_m = \langle \omega_m^a, \omega_m^p, \omega_m^n \rangle$ , and  $\omega_m^p$  and  $\omega_m^n$  are model parameters associated with the agents in physical layer and

network layer, respectively, as will be illustrated later.

(2) *Physical layer agent (pAgent)*: This corresponds to the agent that can interact and adapt to the physical layer environments. For example, a pAgent deployed at the gNB or UE in a mobile network can develop a model to estimate the spectrum availability, and in some cases, keep track of the channel state information (CSIs) of the uplink and downlink channels, and adopt an action function to make recommendations in transmitter and receiver parameter choices, such as bandwidth and channel selections. Similar to the aAgent, we can also define a pAgent by a tuple  $\mathcal{G}^p = \langle \mathcal{A}^p, \mathcal{S}^p, \Gamma^p, \mathcal{D}^p \rangle$  where  $\mathcal{A}^p$  is the action space,  $\mathcal{S}^p$  is the environmental state space, and  $\Gamma^p$  is the set of task-related loss functions, and  $\mathcal{D}^p$  is the set of data samples for training the relevant models. Similar to the aAgent, the decision-making process of the pAgent can also be performed by a model parameterized by  $\omega_m^p$  and an action function that can output an action decision based on the model output. We can write the loss function learned by pAgent for task  $m$  as  $\mathcal{L}_m^p(\Omega_m, \mathcal{D}^p)$  for  $\mathcal{L}_m^p \in \Gamma^p$ .

(3) *Network layer agent (nAgent)*: This corresponds to the agent that interacts with the network layer environments. For example, an nAgent deployed in the transportation layer or the core network of a mobile networking system can keep track of the routing and bandwidth resources between any network entities connecting the UE and its intended destination and adjust the routing and the amount of bandwidth resources accordingly. We define an nAgent by a tuple  $\mathcal{G}^n = \langle \mathcal{A}^n, \mathcal{S}^n, \Gamma^n, \mathcal{D}^n \rangle$  where  $\mathcal{A}^n$  is the set of acts that can be taken by the nAgent,  $\mathcal{S}^n$  is the set of network layer environmental states for an nAgent to estimate and decide its act,  $\mathcal{L}^n$  is the set of task-related loss functions, and  $\mathcal{D}^n$  is the set of data samples for constructing the nAgent's model. Let  $\omega_m^n$  be the model parameters associated with the nAgent. We can write the loss function associated with task  $m$  of pAgent as  $\mathcal{L}_m^n(\Omega_m, \mathcal{D}^n)$  for  $\mathcal{L}_m^n \in \Gamma^n$ .

We can observe that different types of agents generally have different local data modalities, optimization objectives, and models. The traditional way of developing AI models for multi-layer/multi-objective problems often involves training either distinct, task-specific models for individual layers or a single, monolithic foundation model for all three layers. Although the former offers high fidelity for each objective in each layer, it incurs significant computational and storage overheads due to redundant training and deployment. Conversely, the latter may struggle to tailor its output to the nuanced, objective-specific requirements of each layer of the objective.

### 3.2 Problem Formulation

As mentioned earlier, each agent is an independent decision maker, and therefore, the agent controller cannot directly control the decision-making processes of the agents. It can only choose a specific subset of agents when a certain task demand is detected, and then coordinate the local decision-making processes of the selected agents for the task demand of the user. The multi-agent cross-layer optimization problem can be defined as follows:

$$\mathbf{P1:} \min_{\Omega_m} \mathcal{L}_m(\Omega_m) := \langle \mathcal{L}_m^a(\Omega_m, \mathcal{D}^a), \mathcal{L}_m^p(\Omega_m, \mathcal{D}^p), \mathcal{L}_m^n(\Omega_m, \mathcal{D}^n) \rangle.$$

Note that, different from the previous works focusing on finding the global optimization solution to minimize a single objective function, e.g., the weighted sum of local losses of all agents, the optimization objective of problem **P1** involves a vector of objectives from different agents that are associated with different layers of the mobile system. In this case, it is generally impossible to find a single global optimal solution that minimizes the loss functions of all the agents. To address this issue, in this paper, we consider the Pareto optimal solution, a metric commonly adopted for evaluating the tradeoff among a collection of possibly conflicting goals and objectives. More formally, we define the Pareto optimal solution for the multi-agent AgentNet system as follows:

*Definition 1.* A solution profile  $\Omega$  is called *Pareto stationary solution* if there exists a set of non-negative weights  $\gamma^a$ ,  $\gamma^p$ , and  $\gamma^n$  such that  $\sum_{i \in \{a, p, n\}} \gamma^i = 1$  and  $\sum_{i \in \{a, p, n\}} \gamma^i \nabla \mathcal{L}_m^i(\Omega, \mathcal{D}^i) = 0$ . A solution profile  $\Omega^*$  is *Pareto optimal* if no other Pareto stationary solution  $\Omega$  for  $\Omega \neq \Omega^*$  such that  $\mathcal{L}_m^i(\Omega) \leq \mathcal{L}_m^i(\Omega^*, \mathcal{D}^i)$  for all  $i \in \{a, p, n\}$  and  $\mathcal{L}_m^i(\Omega) < \mathcal{L}_m^i(\Omega^*, \mathcal{D}^i)$  for at least one  $i \in \{a, p, n\}$ .

From the above definition, we can observe that the Pareto stationary solution seeks a feasible solution set in which no other feasible solution can improve one agent's objective without causing a deterioration in at least one other agent's objective. In other words, in a Pareto stationary solution, there is no common descent direction for the selected agents in which all the gradients  $\nabla \mathcal{L}_m^i(\Omega_m, \mathcal{D}^i)$  have negative inner products with  $\gamma_m^i$  for all  $i \in \{a, p, n\}$ . Suppose all the loss functions  $\mathcal{L}_m^i(\Omega_m, \mathcal{D}^i)$  for  $i \in \{a, p, n\}$  are smooth and differentiable, a necessary condition for  $\Omega$  to be Pareto stationary is that the convex hull of all gradients  $\langle \nabla \mathcal{L}_m^a(\Omega_m, \mathcal{D}^a), \nabla \mathcal{L}_m^p(\Omega_m, \mathcal{D}^p), \nabla \mathcal{L}_m^n(\Omega_m, \mathcal{D}^n) \rangle$  contains the origin, which means there exist non-negative weights  $\gamma_m^a$ ,  $\gamma_m^p$ , and  $\gamma_m^n$  such that  $\sum_{i \in \{a, p, n\}} \gamma_m^i \nabla \mathcal{L}_m^i(\Omega_m, \mathcal{D}^i) = 0$ . In a more general setting, the minimum norm of the weighted sum of gradients, defined as

$$\min_{\gamma_m^i, \forall i \in \{a, p, n\}} \sum_{i \in \{a, p, n\}} \gamma_m^i \nabla \mathcal{L}_m^i(\Omega_m, \mathcal{D}^i) \quad (1)$$

has been commonly considered as the main measure of the Pareto stationary solution.

## 4 MULTI-AGENT OPTIMIZATION OBJECTIVES

Since the main focus of AgentNet-based networking systems is no longer maximizing the volume of transported data packets throughout the network, traditional metrics such as data rate and bit/symbol-error-rate will be insufficient for evaluating its performance. In the remainder of this paper, we consider the following different but correlated performance metrics to investigate the collaborative performance of AgentNet systems.

### 4.1 Objective Optimization Error (O-error)

The main objective of each agent is to optimize its local objective, i.e., minimizing its local loss function. We assume that each agent employs a stochastic gradient descent (SGD)-based approach to train its local model. We can then evaluate the optimization performance of an individual

agent's model based on the gradient of its local loss function, calculated based on its locally collected dataset. More specifically, we define the optimization error of individual agent  $i$  when being selected for task  $m$  as follows:

*Definition 2.* The optimization error (O-error) of an individual agent  $i$  for  $i \in \{a, n, p\}$  to perform task  $m$  based on dataset  $\mathcal{D}^i$  is defined as

$$\mathcal{E}_O^i = \|\nabla \mathcal{L}_m^i(\boldsymbol{\omega}_m^i, \mathcal{D}^i)\|. \quad (2)$$

Suppose a set of agents,  $\mathcal{T}$ , has been selected to execute the same task  $m$ . We define the joint optimization error (O-error) as

$$\mathcal{E}_O = \left\| \sum_{i \in \{a, p, n\}} \gamma_m^i \nabla \mathcal{L}_m^i(\boldsymbol{\Omega}_m, \mathcal{D}^i) \right\|. \quad (3)$$

where  $\gamma_m^i$  is the weighting coefficient that reflects the influence of each individual objective's learning direction on the overall optimization process. Generally speaking, the weighting coefficients of different agents need to be carefully selected to achieve a robust and well-rounded balance among different agents' objectives towards the user's overall semantic goal.

## 4.2 Generalization Error (G-error)

We also consider the agent's generalization capability when being deployed in an open dynamic environment that cannot be fully captured by its local training dataset. Specifically, we adopt a commonly adopted metric to quantify the generalization capability of each agent, defined as follows:

*Definition 3.* We define the generalization error (G-error) as the discrepancy between the agent deployment performance based on the real data distribution and the training performance obtained on the training dataset. More formally, let  $\tilde{\mathcal{L}}_m^i(\boldsymbol{\omega}_m^i)$  be the population loss of the agent  $i$ 's model for  $i \in \{a, n, p\}$ , evaluated over the real data distribution of task  $m$ . We can then define G-error of agent  $i$ 's model  $\mathcal{E}_G^i$  as the difference of the gradients between the population loss  $\tilde{\mathcal{L}}_m^i(\boldsymbol{\omega}_m^i)$  calculated based on the real distribution of agent deployment and the empirical loss  $\mathcal{L}_m^i(\boldsymbol{\omega}_m^i, \mathcal{D}^i)$  obtained based on the training dataset  $\mathcal{D}^i$ , i.e., the G-error of agent  $i$  can be written as:

$$\mathcal{E}_G^i = \|\nabla \mathcal{L}_m^i(\boldsymbol{\omega}_m^i, \mathcal{D}^i) - \nabla \tilde{\mathcal{L}}_m^i(\boldsymbol{\omega}_m^i)\|, \quad (4)$$

Similar to the O-error, when a set of agents,  $\mathcal{T}$ , has been selected to act collaboratively for the same task  $m$ , we define the generalization error of a collaborative set of agents as follows:

$$\mathcal{E}_G = \left\| \sum_{i \in \{a, p, n\}} \gamma_m^i (\nabla \mathcal{L}_m^i(\boldsymbol{\Omega}_m, \mathcal{D}^i) - \nabla \tilde{\mathcal{L}}_m^i(\boldsymbol{\Omega}_m)) \right\|, \quad (5)$$

## 4.3 Multi-objective Conflicting Error (C-error)

As mentioned earlier, one of the key differences between AgentNet and the traditional centralized networking system is that, in AgentNet, each individual agent focuses on optimizing its own objective, and different objectives of different agents may conflict with each other. We can therefore introduce the following metric to quantify the

performance degradation caused by conflicting objectives among different agents.

*Definition 4.* We define the (multi-agent objective) conflicting error (C-error) as the error caused by the conflicting gradients among different agents, defined as follows:

$$\mathcal{E}_C := \left\| \sum_{i \in \{a, p, n\}} (\gamma_m^i - \gamma_m^{i*}) \nabla \mathcal{L}_m^i(\boldsymbol{\Omega}_m, \mathcal{D}^i) \right\|, \quad (6)$$

where  $\gamma_m^{i*}$  denotes the optimal weight of the agent  $i$  for task  $m$ .

## 5 SANET ARCHITECTURE AND OPTIMIZATION ALGORITHMS

### 5.1 Architecture Overview

We propose SANet, a semantic-aware AgentNet framework that supports multi-agent/multi-objective cross-layer optimization.

The workflow of the SANet is described as follows: **(1) Semantic-aware task/goal cognition:** A set of prompts that reflects the key semantic intent of the users is predefined and can be recognized by an interface deployed at the UE to capture the user's input. The user's input involving these key prompts will be tokenized and converted into low-dimensional embeddings to be sent to the agent controller. The agent controller leverages an LLM-based interface to identify the user's semantic goal, which is then linked to a specific task  $m$  in a finite task space  $\mathcal{M}$ . **(2) Agent selection and model partition:** The agent controller will reason about the appropriate model architecture and logically break down the identified task goal into a set of discrete subtasks, each can be solved by an individual agent. A set of agents that can solve the identified subtasks will then be selected to solve the task goal. In this case, each agent will be assigned a specific loss function corresponding to a particular sub-task. **(3) Multi-agent model partition and sharing:** The agent controller will learn the parameters of the shared-part model according to the identified task and the capabilities of the selected agents. The agent-specific part of the model parameters will be learned by each agent during the model training. **(4) Collaborative inference:** After the model training process, each agent will send its model output to the agent controller based on its local input. The agent controller will then output the final results of the selected agents, which will then be sent back to the agents to decide their actions. The agent controller will evaluate the performance and completeness of the users' goals based on the output results.

We describe the multi-agent model training and inference in detail as follows:

### 5.2 Multi-agent Model Partition and Sharing

We propose a novel multi-agent model partition and sharing (MoPS)-based framework for collaborative model construction in which multiple large models, e.g., deep learning models, deployed at different agents for different subtasks can be partitioned into *shared-part* and *agent-specific part* according to the computational resource constraints of different agents. More specifically, in MoPS, the agent controller

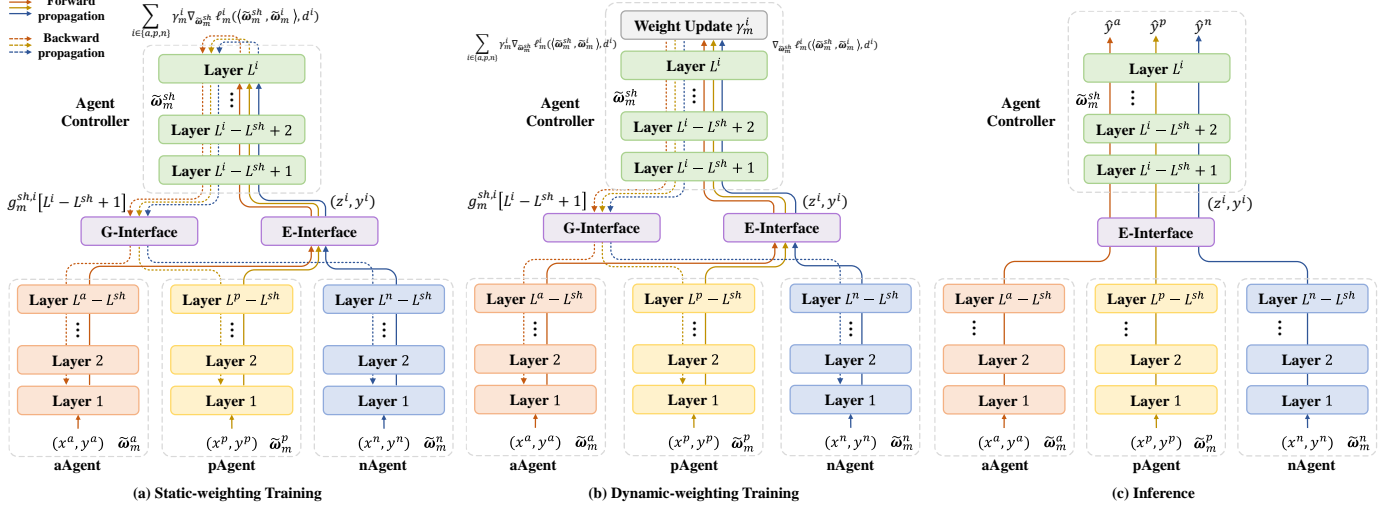


Fig. 3: Model training procedures of (a) static-weighting and (b) dynamic-weighting algorithms, and (c) inference procedures of both algorithms.

hosts the shared-part model's parameters, forming a common foundation for all subtasks, and each individual agent, constrained by its local computational capacity, receives a carefully selected, localized part of the model parameters, trained exclusively on the agent's local dataset for the targeted subtasks. MoPS leverages available resources at the agents efficiently, avoiding the need for each agent to process the entire model. Our proposed framework is scalable and applicable to large AgentNet systems, composed of diverse agents implemented in complex environments.

More formally, suppose each agent  $i$  needs to construct an  $L_i$ -layered model for executing its assigned subtask, in which  $L^{sh}$ -layered shared-part model parameterized by  $\tilde{\omega}_m^{sh}$  is deployed at the agent controller and the rest ( $L^i - L^{sh}$ )-layered agent-specific model parameterized by  $\tilde{\omega}_m^i$  is deployed locally, for  $L^{sh} \leq L^i, \forall i \in \{a, p, n\}$ . Note that the number of layers of agent-specific part models can be different at different agents, i.e.,  $L^i \neq L^j$  for  $i \neq j$  and  $i, j \in \{a, p, n\}$ . In this case, the local loss function of each agent  $i$  can be written as  $\mathcal{L}_m^i(\langle \tilde{\omega}_m^{sh}, \tilde{\omega}_m^i \rangle, \mathcal{D}^i)$  where  $\omega_m^i = \langle \tilde{\omega}_m^{sh}, \tilde{\omega}_m^i \rangle$  and  $\mathcal{D}^i$  is its local dataset.

The optimization problem **P1** can then be rewritten in the following form:

$$\mathbf{P2:} \min_{\langle \tilde{\omega}_m^{sh}, \tilde{\omega}_m^a, \tilde{\omega}_m^p, \tilde{\omega}_m^n \rangle} \left\| \sum_{i \in \{a, p, n\}} \gamma_m^i \nabla \mathcal{L}_m^i(\langle \tilde{\omega}_m^{sh}, \tilde{\omega}_m^i \rangle, \mathcal{D}^i) \right\|^2. \quad (7)$$

Before we describe the detailed model training and inference procedures to solve the above problem, let us introduce the interface for privacy-preserving coordination among different types of agents. Since agents cannot expose their local datasets, but can coordinate their local learning and inference process based on their intermediate model output embeddings and the gradients, we introduce the following two types of interfaces for coordinating the intermediate embeddings and gradients for multi-agent collaborative model training and inference:

- (1) *E-interface (Embedding coordination interface)*: The E-interface establishes a standardized, fixed-size vector space, ensuring that the rich, high-dimensional

representations output by partial models at different agents are compatible with each other for the joint model training and inference. In particular, E-interface specifies a specific protocol for data serialization and numerical normalization to manage disparate output formats and scales of different agents. More specifically, let  $f_{\tilde{\omega}_m^i}(\cdot)$  be the mapping function that maps any input data sample into the final layer output embedding of the model with parameter  $\tilde{\omega}_m^i$ . In our proposed MoPS framework, each agent will not upload any local data samples, but can periodically coordinate with others by uploading a batch of embedding-label pairs  $\langle z_k^i, y_k^i \rangle$  to the agent controller, where  $z_k^i = f_{\tilde{\omega}_m^i}(x_k^i)$  is the final layer output embedding of the model with parameter  $\tilde{\omega}_m^i$  by passing the input data  $x_k^i$  through it, and  $y_k^i$  is the label.

- (2) *G-interface (Gradient coordination interface)*: G-interface, which complements the E-interface, is necessary for coordinating the learned gradients of subtask specific losses among agents. Unlike the E-interface, which is primarily designed for inference, the G-interface regularizes the coordination during multi-agent model training. The interface defines a clear and consistent structure for gradient tensors, regardless of the local model's complexity or the specific objective function being used. In our proposed MoPS framework, after receiving the embedding-label pair  $\langle z_k^i, y_k^i \rangle$  from each agent  $i$ , the agent controller will update the shared-part model  $\tilde{\omega}_m^{sh}$  by calculating the corresponding gradient  $\nabla_{\tilde{\omega}_m^{sh}} \ell_m^i(\langle \tilde{\omega}_m^{sh}, \tilde{\omega}_m^i \rangle, d^i)$  using the backpropagation operation. More formally, we use the subscript  $t$  to denote the model parameters in the  $t$ th round of model coordination. For the  $t$ th round of coordination, let  $g_{m,t}^{sh,i}[L]$  be the  $L$ th-layer gradient tensor calculated by the agent controller during the  $t$ th round of coordination based on the loss function of agent  $i$ , i.e., we

have  $g_{m,t}^{sh,i}[L] = \nabla_{\tilde{\omega}_{m,t}^{sh}[L]} \ell_m^i(\langle \tilde{\omega}_m^{sh}, \tilde{\omega}_m^i \rangle, d^i)$  for  $L^i - L^{sh} + 1 \leq L \leq L^i$ . We also define  $g_{m,t}^i[L']$  as the  $L'$ th-layer gradient tensor of the agent-specific model  $g_{m,t}^i[L'] = \nabla_{\tilde{\omega}_{m,t}^i[L']} \ell_m^i(\langle \tilde{\omega}_m^{sh}, \tilde{\omega}_m^i \rangle, d^i)$  calculated during the  $t$ th round of coordination for  $1 \leq L' \leq L^i - L^{sh}$ . At the end of the  $t$ th coordination, the controller will distribute the  $g_{m,t}^{sh,i}[L^i - L^{sh} + 1]$  to each agent  $i$  via the G-interface.

Let us now describe the multi-agent gradient descent algorithm that can solve problem **P2** as follows: We consider  $T$  rounds of collaborative model training among a set of selected agents  $\{a, p, n\}$  to meet the demand of the user's task  $m$ . During each round of training, each agent will first update the agent-specific part model based on its local dataset and then coordinate with the agent controller to update the shared-part model. More formally, at the beginning of the  $t$ th round of coordination, we assume the agent controller has already deployed the shared part of the model  $\tilde{\omega}_m^{sh}$  and assigned the subtask-specific part model  $\tilde{\omega}_{m,t}^i$  to each agent  $i$ . Then, during the  $t$ th round of coordination, the following steps are sequentially executed by the agents and the agent controller:

**(1) Local model updating (at each agent):** Each agent  $i$  first downloads the gradient tensor  $g_{m,t-1}^{sh,i}[L^i - L^{sh} + 1]$  from the agent controller via G-interface. It then computes the gradient of its local model parameters based on the chain rule as follows:

$$\begin{aligned} & \nabla_{\tilde{\omega}_{m,t-1}} \ell_m^i(\langle \tilde{\omega}_m^{sh}, \tilde{\omega}_{m,t-1}^i \rangle, d_{t-1}^i) \\ &= \begin{bmatrix} g_{m,t-1}^i[L^i - L^{sh}] \\ g_{m,t-1}^i[L^i - L^{sh} - 1] \\ \dots \\ g_{m,t-1}^i[1] \end{bmatrix} \end{aligned} \quad (8)$$

Agent  $i$  then updates its local model parameter  $\tilde{\omega}_{m,t}^i$  via the standard gradient descent as follows:

$$\tilde{\omega}_{m,t}^i = \tilde{\omega}_{m,t-1}^i - \beta_t \nabla_{\tilde{\omega}_{m,t-1}} \ell_m^i(\langle \tilde{\omega}_m^{sh}, \tilde{\omega}_{m,t-1}^i \rangle, d_{t-1}^i), \quad (9)$$

where  $\beta_t$  is the step size of the model update.

**(2) Embedding uploading (via E-interface):** Each agent  $i$  calculates the model output embedding  $z_t^i = f_{\tilde{\omega}_{m,t}^i}(x_t^i)$  and then uploads the embedding-label pair  $\langle z_t^i, y_t^i \rangle$  to the agent controller via E-interface.

**(3) Shared model updating (at agent controller):** Upon receiving the embedding-label pairs from all called agents, the agent controller updates the shared-part model  $\tilde{\omega}_m^{sh}$  by performing the aggregated gradient descent as follows:

$$\begin{aligned} & \tilde{\omega}_m^{sh} \\ &= \tilde{\omega}_{m,t-1}^{sh} - \beta_t \sum_{i \in \{a, p, n\}} \gamma_m^i \nabla_{\tilde{\omega}_{m,t-1}^{sh}} \ell_m^i(\langle \tilde{\omega}_m^{sh}, \tilde{\omega}_{m,t}^i \rangle, d_t^i) \\ &= \tilde{\omega}_{m,t-1}^{sh} - \beta_t \sum_{i \in \{a, p, n\}} \gamma_m^i \begin{bmatrix} g_{m,t-1}^{sh,i}[L^i] \\ g_{m,t-1}^{sh,i}[L^i - 1] \\ \dots \\ g_{m,t-1}^{sh,i}[L^i - L^{sh} + 1] \end{bmatrix}, \end{aligned} \quad (10)$$

where  $\gamma_m^i$  is the weighting coefficient of agent  $i$ .

**(4) Updated gradient distribution (via G-interface):** The agent controller will calculate the output gradient tensor

$g_{m,t}^{sh,i}[L^i - L^{sh} + 1]$  to be sent to each agent  $i$  via the G-interface.

The above steps will be repeated in each round of coordination until the collaboratively trained model meets the requirements of the user, which can be specified by a combination of performance measures, including O-error, G-error, C-error, and R-cost, which will be discussed in detail in Section 6.

During the inference phase, each agent will calculate the output embedding of the agent-part model based on the observed data samples and send the embeddings to the agent controller via the E-interface. The agent controller will output the final decisions based on the output of the shared-part model.

Note that, since in the above algorithm, the weighting coefficients of  $\gamma_m^i$  of each agent need to be pre-defined and assumed to be static during the entire training process, we refer to the above algorithm as the static-weighting algorithm. The model training and inference procedures are illustrated in Fig. 3(a) and (c), respectively.

### 5.3 Dynamic Weighting Algorithm for Conflict-resolving

As mentioned earlier, the diverse objectives and data modalities of different subtasks performed by the agents often lead to inherent conflicts. These conflicts arise because the optimization trajectories for different subtasks are not always aligned and can, at times, be opposed, as illustrated in Fig. 1. This conflict is mainly reflected in the shared-part model updated in (10) in which the gradients output of different agent-specific part models are aggregation with each other to update the shared-part model.

Motivated by the fact that the weight of each objective's gradient directly influences the model's overall optimization direction, in this section, we propose a dynamic weighting algorithm in which the weighting coefficients of different agents can be dynamically optimized throughout the training process to resolve conflicts between different objectives. In particular, during each round  $t$  of model training, each agent  $i$  needs to calculate and upload two additional embedding-label pairs, calculated based on two independent data samples denoted by  $d_{t(1)}^i$  and  $d_{t(2)}^i$ , to the agent controller. The agent controller can then update the weighting coefficient  $\gamma_{m,t}^i$  of each agent  $i$  based on the gradients calculated based on these two data samples as follows:

$$\begin{aligned} \gamma_{m,t}^i &= \gamma_{m,t-1}^i - \eta_t \nabla_{\tilde{\omega}_{m,t-1}^{sh}} \ell_m^i(\langle \tilde{\omega}_m^{sh}, \tilde{\omega}_{m,t}^i \rangle, d_{t(1)}^i)^\top \\ &\quad \cdot \nabla_{\tilde{\omega}_{m,t-1}^{sh}} \ell_m^i(\langle \tilde{\omega}_m^{sh}, \tilde{\omega}_{m,t}^i \rangle, d_{t(2)}^i), \end{aligned} \quad (11)$$

where  $\eta_t$  is the step size for weight update. The above weighting coefficient will be substituted into (10) to update the shared-part model. The rest of the algorithm follows the same line as the static-weighting-based solution introduced in the previous section. The inference procedures are the same as the static-weighting algorithm.

We refer to the above algorithm as the dynamic-weighting algorithm. The model training and inference procedures are illustrated in Fig. 3(b) and (c), respectively.

TABLE 1: Theoretical bounds of O-, G-, and C-errors for static- and dynamic-weighting algorithms, where  $T$  denotes the number of coordination rounds,  $D$  the dataset size.  $\mathcal{O}(\cdot)$  denotes the asymptotic upper bound, and  $\Theta(\cdot)$  the asymptotic tight bound.

Algorithm	Static-weighting	Dynamic-weighting
O-Error	$\mathcal{O}((\beta T)^{-\frac{1}{2}} + \beta^{\frac{1}{2}})$	$\mathcal{O}((\beta T)^{-\frac{1}{2}} + \beta^{\frac{1}{2}} + \eta^{\frac{1}{2}})$
G-Error	$\mathcal{O}(T^{\frac{1}{2}} D^{-\frac{1}{2}})$	$\mathcal{O}(T^{\frac{1}{2}} D^{-\frac{1}{2}})$
C-Error	$\Theta(1)$	$\mathcal{O}((\eta T)^{-1} + \beta^{\frac{1}{2}} \eta^{-\frac{1}{2}} + \eta)$

## 6 THEORETICAL ANALYSIS

In this section, we present the theoretical results of O-, G-, and C-errors for both static- and dynamic-weighting algorithms proposed in the previous section. We summarize all the theoretical bounds derived in this section in Table 1.

### 6.1 O-Error

We can prove the following theoretical bound on the O-error for the static-weighting algorithm.

**Theorem 1 (O-error bound of static-weighting algorithm).**

Suppose the following assumptions hold:

*Assumption 1.* For any  $i \in \{a, p, n\}$ ,  $\nabla \ell_m^i(\Omega_m, d^i)$  is  $\mu_g$ -Lipschitz continuous for any data sample, i.e.,  $\|\nabla \ell_m^i(\Omega_m, d^i) - \nabla \ell_m^i(\Omega'_m, d^i)\| \leq \mu_g \|\Omega_m - \Omega'_m\|$ .

*Assumption 2.* For any  $i \in \{a, p, n\}$ ,  $\ell_m^i(\Omega_m, d^i)$  is  $\mu_l$ -Lipschitz continuous for any data sample, i.e.,  $\|\ell_m^i(\Omega_m, d^i) - \ell_m^i(\Omega'_m, d^i)\| \leq \mu_l \|\Omega_m - \Omega'_m\|$ .

*Assumption 3.* For any  $\gamma_m^i, i \in \{a, p, n\}$ , the initialized model  $\Omega_{m,0}$  satisfies that

$$\mathbb{E} \left[ \sum_{i \in \{a, p, n\}} \gamma_m^i \ell_m^i(\Omega_{m,0}, d^i) \right] - \min_{\Omega_m} \mathbb{E} \left[ \sum_{i \in \{a, p, n\}} \gamma_m^i \ell_m^i(\Omega_m, d^i) \right] \leq c_I.$$

Suppose the model  $\{\Omega_{m,t}\}_{t=1}^T$  is trained by the static-weighting algorithm with  $\beta_t = \beta \leq \frac{1}{2\mu_g}$ . We can prove the following result of O-error:

$$\frac{1}{T} \sum_{t=0}^{T-1} \mathbb{E}[\mathcal{E}_{O,t}] \leq \sqrt{\frac{c_I}{\beta T}} + \sqrt{\frac{\beta \mu_g \mu_l^2}{2}}. \quad (12)$$

*Proof:* See Appendix A.2. □

Assumptions 1-3) are commonly introduced for most theoretical analysis of SGD-based AI model training processes and are quite reasonable in many practical scenarios [37], [38]. In particular, these assumptions essentially state that the loss function and its gradient are well-conditioned and the training process starts within a reasonable range. More specifically, Assumptions 1) and 2) imply that the rate of change of the function is bounded, preventing sudden, massive jumps in the loss value for small changes in the model's parameters, i.e., any small adjustments to the model's weights lead to predictable and manageable changes in the loss. These assumptions hold for many popular loss functions such as the mean squared error (MSE) and cross-entropy. Assumption 3) is also a very mild assumption, as the goal of model training is always to

achieve a significant, but bounded, improvement from a randomly selected initial state.

The upper bound in (12) quantifies the joint impact of three key variables on the O-error, including the initially selected model parameters  $\Omega_{m,0}$ , the number of coordination rounds  $T$  among agents, and the learning rate  $\beta$ . For example, if we choose  $\beta = \Theta(T^{-\frac{1}{2}})$ , the O-error converges at the optimal rate of  $\mathcal{O}(T^{-\frac{1}{4}})$ .

We can similarly prove the following theoretical bound on the O-error of the dynamic-weighting algorithm.

**Corollary 1 (O-error bound of dynamic-weighting algorithm).**

Suppose assumptions 1-3 hold. Suppose model  $\{\Omega_{m,t}\}_{t=1}^T$  is trained by the dynamic-weighting algorithm with  $\beta_t = \beta \leq \frac{1}{2\mu_g}, \eta_t = \eta$ . We can prove the following bound:

$$\frac{1}{T} \sum_{t=0}^{T-1} \mathbb{E}[\mathcal{E}_{O,t}] \leq \sqrt{\frac{c_I}{\beta T}} + 3 \sqrt{\frac{\eta \mu_l^4}{2}} + \sqrt{\frac{\beta \mu_g \mu_l^2}{2}}. \quad (13)$$

*Proof:* See Appendix A.3. □

From Corollary 1, we can observe that the dynamic-weighting algorithm results in  $3\sqrt{\frac{\eta \mu_l^4}{2}}$  increase on the upper bound of O-error, compared to the static-weighting algorithm. This is because, in each round of coordination, the dynamic-weighting algorithm requires extra steps to adjust the optimization directions of each agent's loss by updating its weighting coefficient, i.e., in equation (11), for resolving the multi-objective conflicts among agents. In other words, the increase in the O-error of the dynamic-weighting algorithm can be considered as the cost introduced to resolving conflicts. We can also observe that, by carefully choosing  $\beta = \Theta(T^{-\frac{1}{2}})$  and  $\eta = \Theta(T^{-\frac{1}{2}})$ , the dynamic-weighting algorithm can achieve the same order of convergence  $\mathcal{O}(T^{-\frac{1}{4}})$  as the static-weighting algorithm.

### 6.2 G-Error

Before introducing the theoretical bounds of G-error, let us first define the concept of uniform stability as follows.

**Definition 5 (Uniform stability [38]).** A randomized algorithm

$\mathcal{A}$  is  $\epsilon$ -uniformly stable if for any given datasets  $\mathcal{D}$  and  $\mathcal{D}'$  such that  $\mathcal{D}$  and  $\mathcal{D}'$  differ in at most one data sample, the following inequality holds:

$$\sup_{d^i \in \mathcal{D}^i} \mathbb{E}_{\mathcal{A}}[\|\nabla \ell_m^i(\mathcal{A}(\mathcal{D}), d^i) - \nabla \ell_m^i(\mathcal{A}(\mathcal{D}'), d^i)\|^2] \leq \epsilon^2.$$

Uniform stability is an important property for any stable and trainable algorithms, as it suggests that any small change, such as the removal or alteration of a single data sample, results in only a negligible change to the model's output. Most SGD-based algorithms, especially those with regularization, inherently satisfy this property as they always require the result of the learning algorithms, i.e., the learned models, to be robust and less sensitive to individual data samples.

We can prove the following bound of G-error for the static-weighting algorithm.

**Theorem 2 (G-error bound of static-weighting algorithm).**

Suppose the following assumption holds:

**Assumption 4.** The summation of gradients of all agents is upper bounded, i.e.,  $\mathbb{E}[\|\sum_{i \in \{a, p, n\}} \gamma_m^i \nabla \mathcal{L}_m^i(\Omega_m, \mathcal{D}^i)\|^2] \leq G^2$  where  $G$  is any given constant.

Then, for any uniformly stable static-weighting algorithms  $\mathcal{A}_m$ , the G-error is upper bounded by

$$\mathbb{E}[\mathcal{E}_G] \leq 8G\sqrt{\frac{T}{D}} + \sqrt{\frac{V}{D}}, \quad (14)$$

where  $D$  is the total number of data samples in the datasets of all the agents, i.e.,  $D = \sum_{i \in \{a, p, n\}} |\mathcal{D}^i|$ , and  $V$  is the variance of gradients, given by

$$V = \mathbb{E}[\|\sum_{i \in \{a, p, n\}} \gamma_m^i (\nabla \ell_m^i(\mathcal{A}_m(\mathcal{D}), d^i) - \mathbb{E}[\nabla \ell_m^i(\mathcal{A}_m(\mathcal{D}), d^i)])\|^2].$$

where  $\mathcal{A}_m(\mathcal{D})$  is the model learned by algorithm  $\mathcal{A}_m$  based on dataset  $\mathcal{D}$ .

*Proof.* See Appendix B.2.  $\square$

Inequality (14) quantifies the impact of the number of coordination rounds  $T$  and the size of the dataset  $D$  on the G-error. We can observe that the generalization performance of algorithms generally increases with the size of the dataset and decreases with the total number of coordination rounds. This is because increasing  $T$  beyond a certain point can lead to overfitting, causing the model to memorize the specific non-generalizable features of the training data, thereby degrading its performance on unseen data that exhibit different features than the training dataset. On the other hand, for a fixed number of coordination rounds, increasing the size of the training dataset improves generalization performance by exposing the model to a wider variety of data, which reduces the influence of any single data point and encourages the learning of more robust, universal features.

We can similarly derive the following theoretical bounds of the dynamic-weighting algorithm.

**Corollary 2 (G-error bound of dynamic-weighting algorithm).** Suppose the Assumption 4 holds. Then, the G-error of the dynamic-weighting algorithm is upper bounded by

$$\mathbb{E}[\mathcal{E}_G] \leq 8G\sqrt{\frac{T}{D}} + \sqrt{\frac{V}{D}}. \quad (15)$$

*Proof.* See Appendix B.3.  $\square$

We can observe that the theoretical bound of the dynamic-weighting algorithm is exactly the same as that of the static-weighting algorithm. This means that the extra steps for optimizing the weighting coefficients to resolve the conflicts among different agents cannot affect the generalization performance of the algorithm.

### 6.3 C-Error

We can prove the following result for the C-error of the static-weighting algorithm.

**Theorem 3 (C-error bound of static-weighting algorithm).**

Suppose Assumption 1 holds. Then, there exists a set of static weighting  $\langle \gamma_m^a, \gamma_m^p, \gamma_m^n \rangle$  such that

$$\mathbb{E}[\mathcal{E}_C] = \Theta(1), \quad (16)$$

where  $\Theta(\cdot)$  is the asymptotic tight bound and  $\Theta(1)$  means that the C-error remains a constant as other

variables, such as the number of coordination rounds and the size of the dataset, change.

*Proof.* See Appendix C.2.  $\square$

The above result suggests that the performance degradation caused by conflicting objectives of different agents is fixed with any given weighting coefficients and cannot be alleviated during the model training.

We can prove the following upper bound on the C-error of the dynamic-weighting algorithm.

**Theorem 4 (C-error bound of dynamic-weighting).** Suppose the Assumptions 1 and 2 hold. If the learning rate satisfies  $\beta_t \leq \beta$  and  $\eta_t \leq \eta$ , the following upper bound on the C-error holds for the dynamic-weighting algorithm:

$$\frac{1}{T} \sum_{t=1}^{T-1} \mathbb{E}[\mathcal{E}_{C,t}] \leq \frac{4}{\eta T} + 6\sqrt{3\mu_g\mu_t^2\frac{\beta}{\eta}} + 3\eta\mu_t^4. \quad (17)$$

*Proof.* See Appendix C.3.  $\square$

Inequality (17) quantifies the impact of the number of coordination rounds and learning rate on the C-error of the dynamic-weighting algorithm. We can observe that the C-error reduces with the number of coordination rounds. Also, if we set  $\beta = \Theta(T^{-\frac{3}{4}})$  and  $\gamma = \Theta(T^{-\frac{1}{4}})$ , the C-error can converge at the fastest rate of  $\mathcal{O}(T^{-\frac{1}{4}})$ .

### 6.4 Three-way Tradeoff among O-error, G-error, and C-error

From the results in Theorems 1 to 2, we can observe that the O-, G-, and C-errors are closely related to each other. In particular, from Theorems 1 and 2, we can observe a fundamental tradeoff between O-error and G-error with any given training dataset, i.e., as the number of coordination rounds  $T$  increases, the O-error (or G-error) decreases (or increases). This observation is consistent with previous results about the generalization and optimization tradeoff, or bias-variance tradeoff, which suggests that any model that fits a given set of training data too perfectly will result in poor performance on new unseen data samples [39].

From Theorem 4, we can observe that the C-error in the dynamic-weighting algorithm is also closely linked to the O-error. As mentioned earlier, O-error reduces with the highest rate when the learning rate can be set to  $\beta = \Theta(T^{-\frac{1}{2}})$  and  $\eta = \Theta(T^{-\frac{1}{2}})$ , while the highest convergence rate of C-error requires the learning rates to satisfy  $\beta = \Theta(T^{-\frac{3}{4}})$  and  $\gamma = \Theta(T^{-\frac{1}{4}})$ . This means that the learning rates need to be carefully decided to balance the C-error and O-error with fixed numbers of coordination rounds and dataset sizes.

## 7 PROTOTYPE AND EXPERIMENTAL SETUP

We developed a SANet prototype based on an open-source RAN and softwareized 5G core network, as shown in Fig. 4. In the rest of this section, we first introduce the details of our prototype platform and then present the experimental setup and datasets used in our experiments. Detailed experimental results are presented in the next section.

**Prototype:** The SANet prototype hardware consists of three major components: the gNodeB (gNB), the user equipment (UE), and the 5G core (5GC) network, as illustrated in

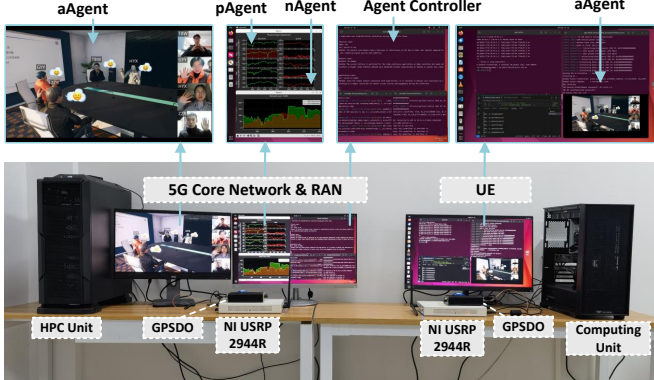


Fig. 4: SANet prototype.

Fig. 4. Specifically, the gNB—which handles all Radio Access Network (RAN) functions—is instantiated using the srsRAN open-source software suite [40]. This software-defined gNB connects to the UE via a Universal Software Radio Peripheral (USRP), NI USRP 2944R, which provides the essential hardware interface for over-the-air communication. The 5GC is implemented entirely using the Open5GS project installed on a workstation equipped with an Intel(R) Core(TM) i9-13900K CPU@5.8GHz, 128GB of DDR5 RAM, and an NVIDIA GeForce RTX 4090 GPU. le environment for evaluating network performance and developing new functionalities.

**Agent Controller:** We installed Qwen-7B [41], an open-source LLM, for reasoning and OpenManus [42] for task separation at the agent controller deployed at the 5GC. We consider two types of events that the agent controller can cognize to trigger the task separation and multi-agent collaborative learning: (1) key prompt detection and (2) traffic and environmental dynamics. In the former case, a set of key prompts related to the specific task demands of the user is predefined and installed at the UE and agent controller. The UE will keep track of the input of the user and, once a key prompt is detected, it will convert it into embeddings to be sent to the agent controller. In the second case, if the current traffic and environmental dynamics result in performance degradation exceeding a maximum tolerable level, i.e., O-error, G-error, and/or C-error exceeds a threshold, the agent controller will initiate the model updating process.

**Agents:** We developed an immersive 3D video conference application based on the SF3D 2D-to-3D video construction model and the Unity 3D rendering engine. This system consists of client applications installed at the UEs and user devices connected to the Internet to stream 2D videos generated by the users and an application server installed at the 5GC to convert the users' 2D videos into corresponding 3D avatars in a virtual conference. The 3D video generated by the application server will be streamed back to the users to offer an immersive 3D conference experience. The agent controller coordinates aAgent, nAgent, and pAgent according to different users' semantic demands. For example, the prompts relevant to users' satisfaction with the streamed video quality, e.g., current video resolution, can be predefined, and if it detects that a user is unsatisfied with the current resolution of the streamed 3D video, the agent

TABLE 2: Hyperparameter Setup

Configuration	Value
Number of coordination rounds $T$	1,000
Step size of model update $\beta$	$5 \times 10^{-4}$
Step size of weight update $\eta$	0.1
Number of encoder/decoder layers	6
Number of attention heads	8
Embedding dimension	128
Model dimension	256
Observation window $x^i$ (s)	15
Prediction window $y^i$ (s)	5

controller will separate the task demand into different requirements at the application layer, physical layer, and network layer and then reason about different steps and model separation and sharing schemes to meet the user's demand. In particular, if the detected semantic demand of the user is to increase the resolution of the streamed 3D video, the agent controller will select an aAgent associated with the demand requesting user to evaluate the required data rates generated by the application server for supporting a higher resolution video streaming, as well as a pAgent to estimate the required physical layer spectrum and the channel CSI and an nAgent to analyze the required network bandwidth to support the required data rates between the application server and client. We develop three different agents: aAgent, pAgent, and nAgent, all of which consist of Transformer-based time-series prediction models and action functions to select the parameters associated with application layer, physical layer, and network layer, respectively, e.g., aAgent, pAgent, and nAgent consist of models to predict the future application-generated data rates, CSIs of different subcarriers between the UE and gNB, and network bandwidths to support the 5G compatible data transmissions, as well as action functions to select the appropriate video streaming resolution, wireless channels, and network bandwidth according to model outputs, respectively. We consider model partition and sharing among the agent controller, aAgent, nAgent, and pAgent, in which the shared-part model parameters associated with the attention layers shared among different Transformer models of aAgent, nAgent, and pAgent are deployed at the agent controller, and the agent-specific model parameters are modality-specific time-series embedding, position encoding module, and attention layers trained by each individual agent based on its local set and modality of data. The detailed model hyperparameters of the agent controller and agents are summarized in Table 2.

## 8 EXPERIMENTAL RESULTS

### 8.1 Multi-agent Model Partition and Sharing

To evaluate the impact of different model partition and sharing schemes on the optimization and generalization performance of AgentNet, we compare the following different partition and sharing schemes and evaluate their performance based on the metrics introduced in Section 4: **Scheme 1 (No sharing):** Each agent trains an independent model based on its local data, and the agent controller does not host any model parameters.

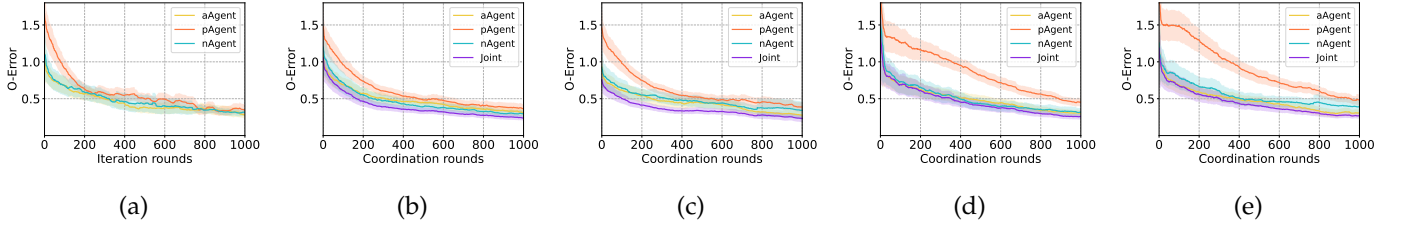


Fig. 5: O-error of different agents using MoPS with (a) Scheme 1, (b) Scheme 2 and (c) Scheme 3 trained by the static-weighting algorithm and (d) Scheme 2 and (e) Scheme 3 trained by the dynamic-weighting algorithm.

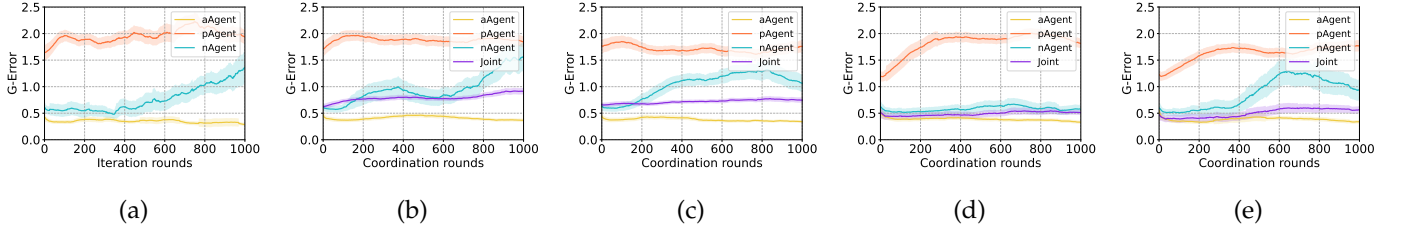


Fig. 6: G-error of different agents using MoPS with (a) Scheme 1, (b) Scheme 2 and (c) Scheme 3 trained by the static-weighting algorithm and (d) Scheme 2 and (e) Scheme 3 trained by the dynamic-weighting algorithm.

**Scheme 2 (Partial sharing I):** Each agent trains a modality-specific time-series embedding and position encoding module, and the agent controller hosts all the Transformer layers (including 6 encoder/decoder layers each with 8 self-attention heads) shared by all agents.

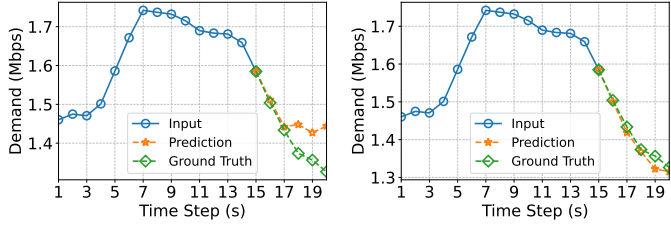
**Scheme 3 (Partial sharing II):** Each agent trains a modality-specific time-series embedding and position encoding module and the first 6 encoder layers. The agent controller hosts the remaining 6 decoder layers that are shared among all agents.

We present the O-error and G-error of all the above schemes trained based on static-weighting and dynamic-weighting algorithms under different numbers of coordination rounds in Fig. 5 and 6, respectively. We can observe that, as the number of coordination rounds increases, different agents' O-errors reduce at different rates, especially when trained by the static-weighting algorithm. Disparities in the convergence rates of collaboratively trained agents lead to the divergence, i.e., conflicts, in their respective optimization trajectories, which impede the overall performance of the AgentNet. The G-errors of pAgent and nAgent increase with the number of coordination rounds in both static-weighting and dynamic-weighting algorithms. This aligns with our derived theoretical results in Section 6, which suggests that increasing the coordination round numbers for given datasets will result in improved model fitting and degraded generalization performance for new environments. Note that in Fig. 5 and 6, the pAgent's G-error is generally the largest among all the agents, while its O-error also reduces at the slowest rate and remains in a relatively fixed value when the number of coordination rounds continues to increase. This is because the model training and testing dataset considered in our experiments are collected from the real 5G channel CSI, and generally speaking, the wireless channel exhibits higher randomness and dynamics, compared to the network and application layers. Therefore, it is generally more challenging to construct a time-series prediction model that achieves a relatively good optimization and generaliza-

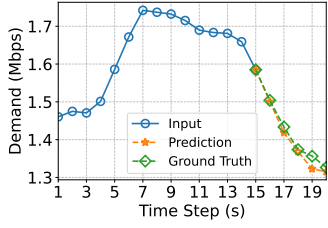
tion performance for wireless CSI signals.

An interesting observation in Fig. 5 and 6 is that allowing partial model sharing among different agents not only enhance the generalization performance, but also improve the optimization performance for each individual agent, e.g., both partial sharing schemes (Schemes 2 and 3) have lower O-error for each agent, compared to the no sharing scheme (Scheme 1) in which each agent trains its local model independently, i.e., Schemes 2 and 3 based on our proposed MoPS provide around 17.61% and 13.87% reduction per agent on O-error and 23.57% and 37.62% reduction on G-error, compared to Scheme 1. In particular, different agents train their models based on different data modalities, and also data samples collected from the physical layer, network layer, and application layer are often assumed to be independent. Our results suggest that even these seemly independent environments may still share some common features. This is aligned with the surprising observation in statistical decision theory, the Stein's paradox [43], suggesting that it is better to simultaneously estimate three or more independent parameters, instead of estimating these parameters separately. The above experimental results further justify the unique advantage of our proposed MoPS for supporting flexible and scalable deployment of large models in resource-limited agents.

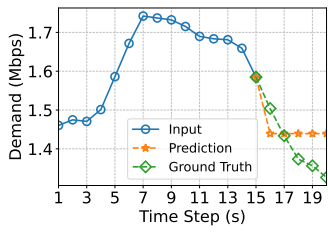
To further verify the improvements on each agent's prediction results by allowing partial model sharing among multiple agents that interact with independent environments, in Fig. 7–9, we compare the prediction accuracy of each agent using MoPS to that of no model sharing, in which each agent trains an independent model using the state-of-the-art time-series prediction algorithms, including LSTM [44], N-BEATS [45], Transformer [46], and Informer [47]. We also present the normalized mean absolute error (NMAE) of the prediction results from different models using the box-and-whisker plot to evaluate their performance. We can observe that MoPS achieves the highest prediction accuracy, i.e., with the lowest median NMAE (the orange line), for



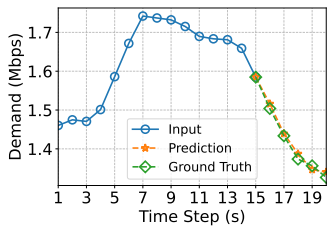
(a)



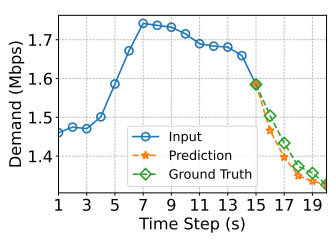
(b)



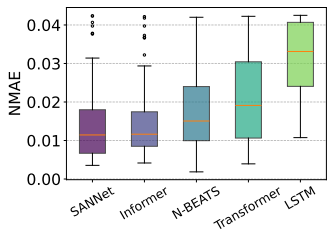
(c)



(d)



(e)

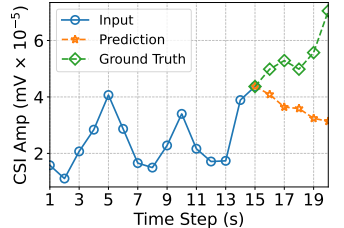


(f)

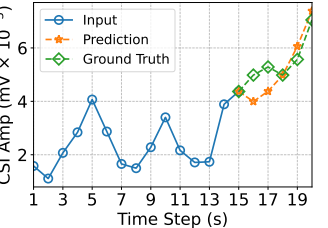
Fig. 7: Prediction of user demand in aAgent based on (a) LSTM, (b) N-BEATS, (c) Transformer, (d) Informer, (e) MoPS, and (f) comparison of different models' prediction performance based on NMAE.

all three agents, e.g., the median NMAE values of MoPS are approximately 0.0109, 0.284, and 0.00267 at the physical, network, and application layers, respectively, corresponding to performance gains of 4.59%, 1.41%, and 14.61%, respectively, compared to the best-performing baseline methods. Also, the MoPS and Informer have relatively smaller variability compared to other models. This means that these two models offer higher consistencies in their prediction results than others.

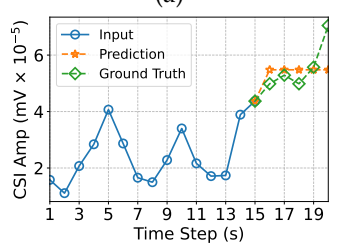
To evaluate the performance of the proposed dynamic-weighting algorithm in reducing the conflicts among different agents with different objective functions, we compare the convergences of loss functions of different agents when being collaboratively trained in Fig. 10 and also present the C-errors of the two partial sharing schemes (Schemes 2 and 3) with static-weighting and dynamic-weighting algorithms in Fig. 11. We can observe that the loss function values of different agents exhibit different dynamics when being trained by the static-weighting algorithm, e.g., the loss values of the pAgent stop decreasing after around 860 rounds of coordination. In the dynamic-weighting algorithm, the loss functions of all the agents converge to a smaller value. The effectiveness of the dynamic-weighting algorithm in resolving conflicts among agents is further verified in Fig. 11, where we can directly observe that the C-errors of both partial sharing schemes (Schemes 2 and 3) trained by the dynamic-weighting algorithm are much lower, i.e., around



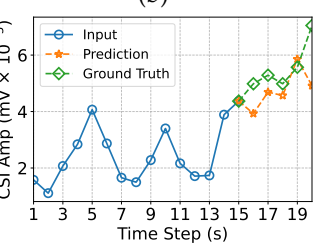
(a)



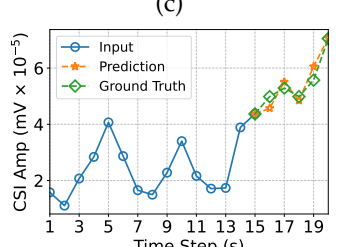
(b)



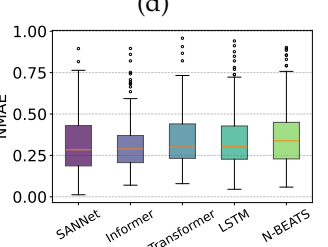
(c)



(d)



(e)



(f)

Fig. 8: Prediction of channel CSIs (n1 band, 2110-2170 MHz) in pAgent based on (a) LSTM, (b) N-BEATS, (c) Transformer, (d) Informer, (e) MoPS, and (f) comparison of different models' prediction performance based on NMAE.

76.60% and 83.81% reductions in Schemes 2 and 3, than those trained by the static-weighting algorithm. We can also observe that the C-error of Scheme 3 is always lower than that of Scheme 2. This is because the shared-part of model parameters hosted by the agent controller mainly captures the common features of different agents' objectives, and therefore, the higher the portion of the shared parameters, the more C-error for the AgentNet.

To evaluate the communication and computational resource consumption of MoPS, we record the number of coordination rounds and the floating-point operations per second (FLOPs) of the agent controller and agents required to achieve a satisfactory O-error, e.g., less than a fixed threshold 0.4, with different MoPS schemes trained by the static-weighting and dynamic-weighting algorithms in Table 3. Note that in our experiments, we adopt the same-sized Transformer model for different agents and, therefore, their required FLOPs are equal. We can observe that increasing the number of shared parameters at the agent controller can significantly reduce the required computational load of each agent. They, however, result in a higher communication cost for both static-weighting and dynamic-weighting algorithms. This is because, as mentioned earlier, allowing more shared-part model parameters generally results in more conflict among different agents, leading to a slower convergence for collaborative training. This observation re-

TABLE 3: Communication and computational resource consumption

Algorithms	MoPS Schemes	Computation (M)		Number of coordination rounds
		a/p/nAgent	Agent Controller	
Static-weighting Training	Scheme 1	116.5	/	/
	Scheme 2	47.9	277.0	651
	Scheme 3	87.3	121.4	690
Dynamic-weighting Training	Scheme 2	158.0	589.5	486
	Scheme 3	276.8	255.1	514
Inference	Scheme 1	31.1	/	/
	Scheme 2	13.8	52.1	/
	Scheme 3	26.7	22.3	/

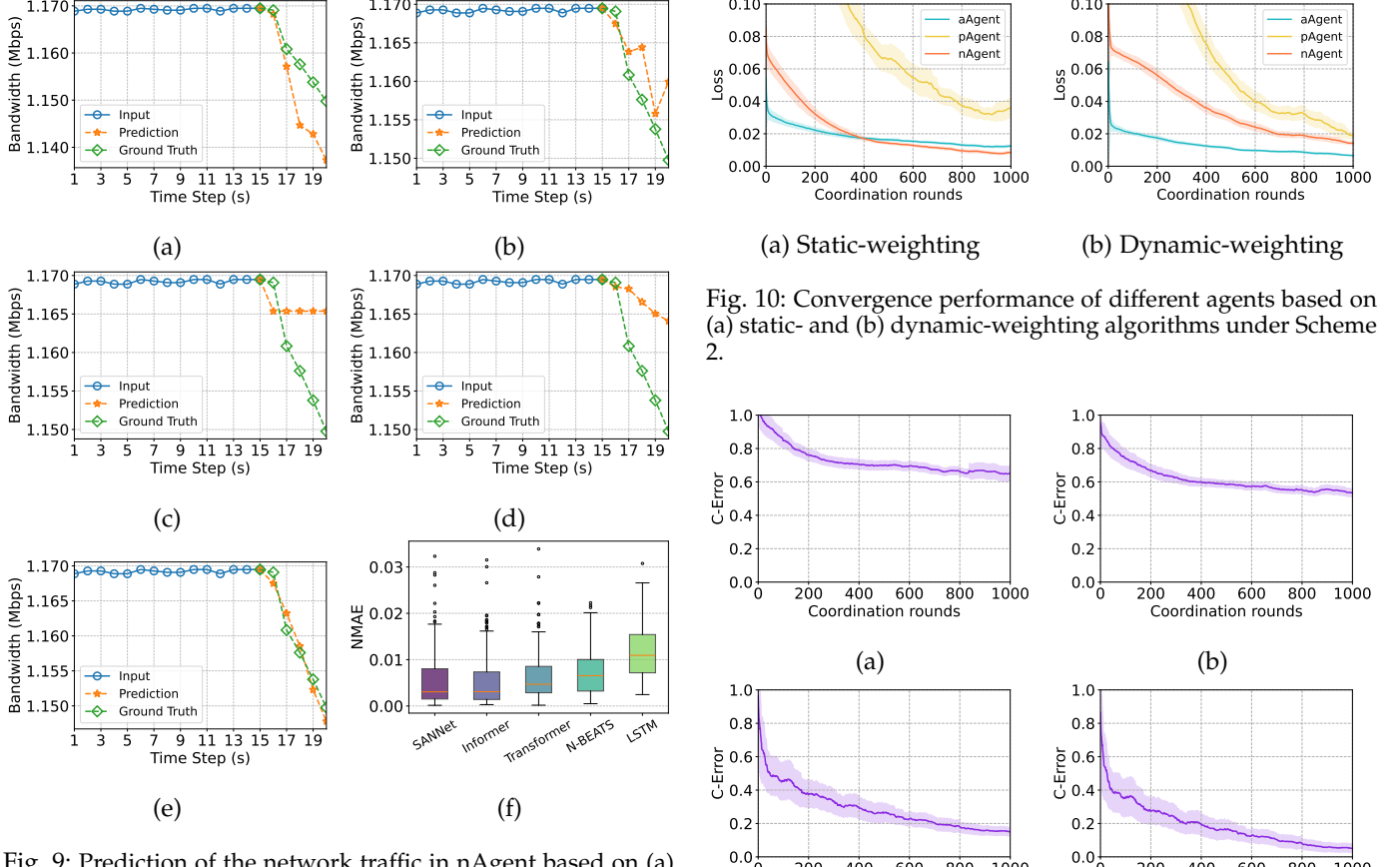


Fig. 9: Prediction of the network traffic in nAgent based on (a) LSTM, (b) N-BEATS, (c) Transformer, (d) Informer, (e) MoPS, and (f) comparison of different models' prediction performance based on NMAE.

veals a tradeoff between the local computation load of each agent and overall communication resources for achieving a specific optimization performance. We also present the resource consumption of the inference phase in Table 3. We can observe that during the inference phase, computational costs are significantly reduced compared to the training phase, e.g., in Scheme 2 (or Scheme 3), the FLOPs of each agent and the agent controller reduce to only 8.73% and 8.84% (or 9.65% and 8.74%) of those required for the training phase, respectively.

## 8.2 Three-way Tradeoff

To verify the three-way tradeoff observed in our theoretical results, we investigate the correlation between G-error, O-error, and C-error for the static-weighting and dynamic-weighting algorithms based on a series of experiments con-

Fig. 10: Convergence performance of different agents based on (a) static- and (b) dynamic-weighting algorithms under Scheme 2.

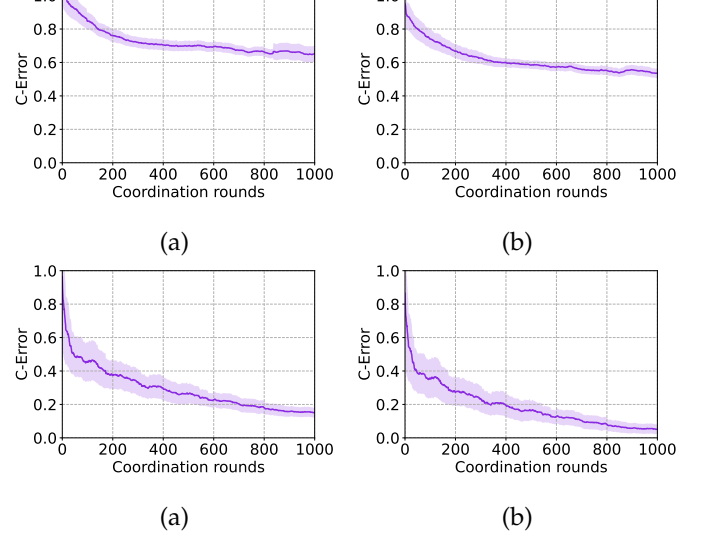


Fig. 11: C-error of MoPS with (a) Scheme 2 and (b) Scheme 3 trained by the static-weighting algorithm and (c) Scheme 2 and (d) Scheme 3 trained by the dynamic-weighting algorithm.

ducted based on our SANet prototype in Fig. 12, where we plot the data points recorded in these experiments into the two-dimensional plane of G-error and O-error as well as that of G-error and C-error. To verify the trends discovered in our theoretical bounds, we first estimate the empirical values of hyperparameters  $\mu_g$ ,  $\mu_l$ ,  $c_I$ , and  $G$  in Theorems 1-4 by fitting the derived mathematical expressions to the experimental data points. We then substitute these estimated empirical values back into the derived mathematical expressions to obtain the theoretical curves, which are plotted in the same two-dimensional plane as the experimental data points, so we can have a direct, visual comparison between the experimental results and the derived theoretical results.

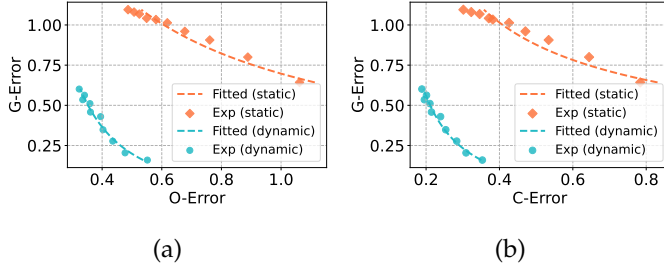


Fig. 12: (a) Tradeoff between G-error and O-error and (b) that between G-error and C-error verified by both theoretical results and experimental results for the static-weighting and dynamic-weighting algorithms.

We can observe that the experimental results match the trend of the theoretical curves, that is, increasing G-error will cause decreases in both O-error and C-error for both the static-weighting and dynamic-weighting algorithms. We can also observe that the dynamic-weighting algorithm can significantly reduce both O-error and C-error for any given G-error value. As mentioned earlier, the dynamic-weighting algorithm requires slightly more computational resources at each agent than the static-weighting algorithm, and is therefore more suitable for the agents with relatively higher computational capacities and more stringent requirements on the generalization and optimization performance.

## 9 CONCLUSION

This paper has proposed SANet, a novel semantic-aware AgentNet architecture that autonomously identifies the user's semantic goal and autonomously divides the identified goal into different subtasks for different agents. We have formulated the decentralized optimization of SANet as a multi-agent multi-objective problem and focus on finding the Pareto optimal solution among agents with distinct and potentially conflicting objectives. Three novel metrics for evaluating the performance of SANet have been proposed: the agents' objective optimization error, dynamic environment generalization error, and multi-objective conflicting error. The MoPS, a model partition and sharing framework, has been proposed in which large models, e.g., deep learning models, of different agents can be partitioned into shared and agent-specific parts that are jointly constructed and deployed according to agents' local computational resources. Two decentralized optimization algorithms, static-weighting and dynamic-weighting algorithms, have been introduced to optimize the proposed metrics. Theoretical bounds for all three performance metrics have been derived. The results have proved that there exists a three-way tradeoff among optimization, generalization, and conflicting errors. Finally, we have developed a SANet prototype, in which three Transformer-based time-series prediction agents have been selected to interact with three different layers of the network system. Experiment results show that the proposed MoPS provides up to 14.61% performance gains with only 44.37% of the Floating-Point Operations (FLOPs) required for inference at each agent compared to state-of-the-art algorithms. Also, the dynamic-weighting algorithm

reduces up to 83.81% training errors caused by conflicting objectives, compared to the static-weighting algorithm.

## REFERENCES

- [1] Y. Xiao, H. Zhou, X. Li, Y. Gao, G. Shi, and P. Zhang, "Sannet: A semantic-aware agentic ai networking framework for multi-agent cross-layer coordination," in *Proceedings of IEEE GLOBECOM*, Taipei, Taiwan, December 2025.
- [2] N. Q. Hieu, D. T. Hoang, D. N. Nguyen, V.-D. Nguyen, Y. Xiao, and E. Dutkiewicz, "Enhancing immersion and presence in the metaverse with over-the-air brain-computer interface," *IEEE Transactions on Wireless Communications*, vol. 23, no. 12, pp. 18 532–18 548, December 2024.
- [3] G. Shi, Y. Xiao, Y. Li, and X. Xie, "From semantic communication to semantic-aware networking: Model, architecture, and open problems," *IEEE Communications Magazine*, vol. 59, no. 8, pp. 44–50, August 2021.
- [4] D. Gunduz *et al.*, "Joint source–channel coding: Fundamentals and recent progress in practical designs," *Proceedings of the IEEE*, pp. 1–32, 2024.
- [5] A. Haque, A. Milstein, and L. Fei-Fei, "Illuminating the dark spaces of healthcare with ambient intelligence," *Nature*, vol. 585, no. 7824, pp. 193–202, September 2020.
- [6] Y. Xiao, G. Shi, and P. Zhang, "Towards agentic AI networking in 6G: A generative foundation model-as-agent approach," *IEEE Communications Magazine*, vol. 63, no. 9, September 2025.
- [7] Y. Xiao, G. Shi, Y. Li, W. Saad, and H. V. Poor, "Toward self-learning edge intelligence in 6G," *IEEE Communications Magazine*, vol. 58, no. 12, pp. 34–40, December 2020.
- [8] Y. Yang *et al.*, "6G network AI architecture for everyone-centric customized services," *IEEE Network*, vol. 37, no. 5, September 2023.
- [9] M. R. Morris *et al.*, "Position: Levels of AGI for operationalizing progress on the path to AGI," in *ICML*, Vienna, Austria, July 2024.
- [10] Y. Shavit, S. Agarwal, M. Brundage, S. Adler, C. O'Keefe, R. Campbell, T. Lee, P. Mishkin, T. Eloundou, A. Hickey *et al.*, "Practices for governing agentic ai systems," *Research Paper, OpenAI*, 2023.
- [11] C. Wu, H. Lu, Y. Chen, and L. Qin, "Cross-layer optimization for statistical qos provision in C-RAN with finite-length coding," *IEEE Transactions on Communications*, vol. 72, no. 6, pp. 3393–3407, Jun. 2024.
- [12] S. He, Z. An, J. Zhu, M. Zhang, Y. Huang, and Y. Zhang, "Cross-layer optimization: Joint user scheduling and beamforming design with qos support in joint transmission networks," *IEEE Transactions on Communications*, vol. 71, no. 2, pp. 792–807, Feb. 2023.
- [13] L.-W. Chien and S.-M. Tseng, "Proximal policy optimization for cross-layer joint design of miso beamforming and ris phase configuration," *IEEE Open Journal of the Communications Society*, pp. 1–1, Jul. 2025.
- [14] K. Han, M. Siew, B. Xu, S. Guo, W. Gong, T. Q. S. Quek, and Q. Ren, "On-demand optimization method for cross-layer topology in multi-task vdeo and mega-leo heterogeneous satellite networks," *IEEE Transactions on Wireless Communications*, pp. 1–1, Jun. 2025.
- [15] T. Taleb, C. Benzaïd, R. A. Addad, and K. Samdanis, "AI/ML for beyond 5G systems: Concepts, technology enablers & solutions," *Computer Networks*, vol. 237, p. 110044, 2023.
- [16] A. AlZailaa, J. Corona, R. Teixeira, H. R. Chi, M. Antunes, A. Radwan, and R. L. Aguiar, "A review of the current usage of ai/ml for radio access network (ran)," *IEEE Access*, 2025.
- [17] H. Zhu *et al.*, "SANSee: A physical-layer semantic-aware networking framework for distributed wireless sensing," *IEEE Transactions on Mobile Computing*, vol. 24, no. 3, pp. 1636–1653, March 2025.
- [18] N. Nurani Krishnan, E. Torkildson, N. B. Mandayam, D. Raychaudhuri, E.-H. Rantala, and K. Doppler, "Optimizing throughput performance in distributed MIMO Wi-Fi networks using deep reinforcement learning," *IEEE Transactions on Cognitive Communications and Networking*, vol. 6, no. 1, pp. 135–150, 2020.
- [19] L. Qin, H. Lu, Y. Chen, B. Chong, and F. Wu, "Toward decentralized task offloading and resource allocation in user-centric mec," *IEEE Transactions on Mobile Computing*, vol. 23, no. 12, pp. 11 807–11 823, 2024.
- [20] M. A. Habibi, B. Han, M. Saimler, I. L. Pavón, and H. D. Schotten, "Towards an AI/ML-driven SMO framework in O-RAN: Scenarios, solutions, and challenges," in *IEEE Future Networks World Forum*, Dubai, UAE, October 2024, pp. 7–14.

[21] A. Ghosh, A. Maeder, M. Baker, and D. Chandramouli, "5G evolution: A view on 5G cellular technology beyond 3GPP release 15," *IEEE Access*, vol. 7, pp. 127 639–127 651, 2019.

[22] X. Lin, "An overview of 5G advanced evolution in 3GPP release 18," *IEEE Communications Standards Magazine*, vol. 6, no. 3, pp. 77–83, 2022.

[23] —, "The bridge toward 6G: 5G-advanced evolution in 3GPP release 19," *IEEE Communications Standards Magazine*, vol. 9, no. 1, pp. 28–35, 2025.

[24] G. Shi and Y. Xiao, "Requirements of semantic-aware networking for future networks," ITU-T TR.Reqts-SAN, Nov. 2023.

[25] —, "An introduction to semantic communication and semantic-aware networking standardization for 6G," *GetMobile: Mobile Comp. and Comm.*, vol. 28, no. 3, p. 14–19, Oct. 2024.

[26] K. B. Letaief, W. Chen, Y. Shi, J. Zhang, and Y.-J. A. Zhang, "The roadmap to 6G: AI empowered wireless networks," *IEEE Communications Magazine*, vol. 57, no. 8, pp. 84–90, August 2019.

[27] R. Sapkota, K. I. Roumeliotis, and M. Karkee, "AI agents vs. agentic AI: A conceptual taxonomy, applications and challenges," *Information Fusion*, vol. 126, p. 103599, 2026.

[28] Z. Durante *et al.*, "Agent AI: Surveying the horizons of multimodal interaction," *arXiv preprint arXiv:2401.03568*, 2024.

[29] J. Wang, H. Xu, H. Jia, X. Zhang, M. Yan, W. Shen, J. Zhang, F. Huang, and J. Sang, "Mobile-agent-v2: Mobile device operation assistant with effective navigation via multi-agent collaboration," in *Proceedings of NeurIPS Conference*, A. Globerson, L. Mackey, D. Belgrave, A. Fan, U. Paquet, J. Tomczak, and C. Zhang, Eds., vol. 37. Curran Associates, Inc., Vancouver, Canada, December 2024, pp. 2686–2710. [Online]. Available: [https://proceedings.neurips.cc/paper\\_files/paper/2024/file/0520537ba799d375b8ff5523295c337a-Paper-Conference.pdf](https://proceedings.neurips.cc/paper_files/paper/2024/file/0520537ba799d375b8ff5523295c337a-Paper-Conference.pdf)

[30] Q. Wang, Z. Wang, Y. Su, H. Tong, and Y. Song, "Rethinking the bounds of LLM reasoning: Are multi-agent discussions the key?" in *Proceedings of the 62nd Annual Meeting of the Association for Computational Linguistics (Volume 1: Long Papers)*, L.-W. Ku, A. Martins, and V. Srikumar, Eds. Bangkok, Thailand: Association for Computational Linguistics, Aug. 2024, pp. 6106–6131. [Online]. Available: <https://aclanthology.org/2024.acl-long.331/>

[31] A. Madaan, N. Tandon, P. Gupta, S. Hallinan, L. Gao, S. Wiegreffe, U. Alon, N. Dziri, S. Prabhumoye, Y. Yang, S. Gupta, B. P. Majumder, K. Hermann, S. Welleck, A. Yazdanbakhsh, and P. Clark, "Self-refine: iterative refinement with self-feedback," in *Proceedings of NeurIPS Conference*, New Orleans, LA, USA, December 2023.

[32] W. Li, Y. Lin, M. Xia, and C. Jin, "Rethinking Mixture-of-Agents: Is mixing different large language models beneficial?" *arXiv preprint arXiv:2502.00674*, February 2025.

[33] S. Chen, L. Zeng, A. Raghunathan, F. Huang, and T. C. Kim, "MoA is all you need: Building LLM research team using mixture of agents," *arXiv preprint arXiv:2409.07487*, September 2024.

[34] J. Wang, J. Wang, B. Athiwaratkun, C. Zhang, and J. Zou, "Mixture-of-Agents enhances large language model capabilities," *arXiv preprint arXiv:2406.04692*, June 2024.

[35] P. Belcak, G. Heinrich, S. Diao, Y. Fu, X. Dong, S. Muralidharan, Y. C. Lin, and P. Molchanov, "Small language models are the future of agentic ai," *arXiv preprint arXiv:2506.02153*, 2025.

[36] D. B. Acharya, K. Kuppan, and B. Divya, "Agentic AI: Autonomous intelligence for complex goals—a comprehensive survey," *IEEE Access*, vol. 13, January 2025.

[37] H. D. Fernando, H. Shen, M. Liu, S. Chaudhury, K. Murugesan, and T. Chen, "Mitigating gradient bias in multi-objective learning: A provably convergent approach," in *Proceedings of ICLR Conference*, Kigali, Rwanda, May 2023.

[38] L. Chen *et al.*, "Three-way trade-off in multi-objective learning: Optimization, generalization and conflict-avoidance," *NIPS*, vol. 36, pp. 70 045–70 093, New Orleans, LA, December 2023.

[39] Z. Yang, Y. Yu, C. You, J. Steinhardt, and Y. Ma, "Rethinking bias-variance trade-off for generalization of neural networks," in *Proceedings of ICML Conference*, Virtual, July 2020, pp. 10767–10777.

[40] srsRAN, "Your own mobile network," <https://www.srslte.com/>, srsRAN, 2019.

[41] J. Bai, S. Bai, Y. Chu *et al.*, "Qwen technical report," *arXiv preprint arXiv:2309.16609*, 2023.

[42] X. Liang, J. Xiang, Z. Yu *et al.*, "OpenManus: An open-source framework for building general AI agents," 2025.

[43] C. Stein, *Inadmissibility of the usual estimator for the mean of a multivariate normal distribution*. University of California Press, 1956, vol. 3.

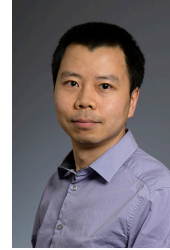
[44] K. Albeladi, B. Zafar, and A. Mueen, "Time series forecasting using LSTM and ARIMA," *International Journal of Advanced Computer Science and Applications*, vol. 14, no. 1, pp. 313–320, 2023.

[45] B. N. Oreshkin, D. Carpov, N. Chapados, and Y. Bengio, "N-beats: Neural basis expansion analysis for interpretable time series forecasting," in *Proceedings of ICLR Conference*, New Orleans, LA, May 2019.

[46] G. Zerveas, S. Jayaraman, D. Patel, A. Bhamidipaty, and C. Eickhoff, "A transformer-based framework for multivariate time series representation learning," in *Proceedings of SIGKDD Conference*, Virtual, August 2021, pp. 2114–2124.

[47] H. Zhou, S. Zhang, J. Peng, S. Zhang, J. Li, H. Xiong, and W. Zhang, "Informer: Beyond efficient transformer for long sequence time-series forecasting," in *Proceedings of AAAI Conference*, vol. 35, no. 12, Virtual, February 2021, pp. 11 106–11 115.

[48] Y. Lei, "Stability and generalization of stochastic optimization with nonconvex and nonsmooth problems," in *Annual Conference on Learning Theory*, Bangalore, India, July 2023, pp. 191–227.



**Yong Xiao** (Senior Member, IEEE) received his B.S. degree in electrical engineering from China University of Geosciences, Wuhan, China in 2002, M.Sc. degree in telecommunication from Hong Kong University of Science and Technology in 2006, and his Ph. D degree in electrical and electronic engineering from Nanyang Technological University, Singapore in 2012. He is now a professor in the School of Electronic Information and Communications at the Huazhong University of Science and Technology (HUST),

Wuhan, China. He is also with Peng Cheng Laboratory, Shenzhen, China, and Pazhou Laboratory (Huangpu), Guangzhou, China. He is the associate group leader of the network intelligence group of IMT-2030 (6G promoting group) and the vice director of 5G Verticals Innovation Laboratory at HUST. Before he joined HUST, he was a research assistant professor in the Department of Electrical and Computer Engineering at the University of Arizona, where he was also the center manager of the Broadband Wireless Access and Applications Center (BWAC), an NSF Industry/University Cooperative Research Center (I/UCRC) led by the University of Arizona. His research interests include machine learning, game theory, distributed optimization, and their applications in agentic AI networking, semantic communications, cloud/fog/mobile edge computing, green networking systems, and Internet-of-Things (IoT).



**Xubo Li** (Student Member, IEEE) received his B.S. degree in biomedical engineering from Huazhong University of Science and Technology, Wuhan, China in 2023. He is currently pursuing his Ph.D. in the School of Electronic Information and Communications at Huazhong University of Science and Technology, Wuhan, China. His research interest includes machine learning, network intelligence, and next-generation wireless communication technology.



**Haoran Zhou** received his B.S. degree in electrical engineering from China University of Geosciences, Wuhan, China, in 2024. He is currently pursuing his Ph.D. in the School of Electronic Information and Communications at Huazhong University of Science and Technology, Wuhan, China. His research interest includes machine learning, network intelligence, and multi-agent communication.



**Yingyu Li** (Member, IEEE) received the B.Eng. degree in electronic information engineering and the Ph.D. degree in circuits and systems from the Xidian University, Xi'an, China, in June 2012 and September 2018, respectively. From September 2014 to September 2016, she was a Research Scholar with the Wireless Networking, Signal Processing and Security Lab, Department of Electronic Computer Engineering, University of Houston, USA. She was a postdoctoral researcher in the School of Electronic Information and Communications at Huazhong University of Science and Technology from October 2018 to November 2021. Since December 2021, she has been an Associate Professor at the School of Mechanical Engineering and Electronic Information, China University of Geosciences (Wuhan). Her research interests include machine learning and artificial intelligence for next-generation wireless networks, federated edge intelligence, green/low-carbon communication networks, distributed optimization, semantic communications, and intelligent Internet of Things.

of Washington, Seattle, USA. Her research interests include modeling and optimization of next-generation mobile communication networks, distributed multiple access, and artificial intelligence for networking.



**Yayu Gao** (Member, IEEE) is an associate professor in the School of Electronic Information and Communications at the Huazhong University of Science and Technology (HUST), Wuhan, China. She received the B.S. degree in electronic engineering from the Nanjing University of Posts and Telecommunications, Nanjing, China, in 2009, and the Ph.D. degree in electronic engineering from the City University of Hong Kong, Hong Kong, China, in 2014. From 2017 to 2018, she was a Visiting Scholar with the University

of Washington, Seattle, USA. Her research interests include modeling and optimization of next-generation mobile communication networks, distributed multiple access, and artificial intelligence for networking.



**Guangming Shi** (Fellow, IEEE) received the M.S. degree in computer control, and the Ph.D. degree in electronic information technology from Xidian University, Xi'an, China, in 1988, and 2002, respectively. He was the vice president of Xidian University from 2018 to 2022. Currently, he is the Vice Dean of Peng Cheng Laboratory and a Professor with the School of Artificial Intelligence, Xidian University. He is an IEEE Fellow, the chair of IEEE CASS Xi'an Chapter, a senior member of ACM and CCF, Fellow of the Chinese Institute of Electronics, and Fellow of IET. He was awarded Cheung Kong Scholar Chair Professor by the Ministry of Education in 2012. He won the second prize of the National Natural Science Award in 2017. His research interests include Artificial Intelligence, Semantic Communications, and Human-Computer Interaction.



**Ping Zhang** (Fellow, IEEE) is a professor in the School of Information and Communication Engineering at the Beijing University of Posts and Telecommunications. He is a member of the National Academy of Engineering of China. He is currently the director of State Key Laboratory of Networking and Switching Technology, a member of IMT-2020 (5G) Experts Panel, and a member of the Experts Panel for China's 6G development. He was the Chief Scientist of the National Basic Research Program (973 Program), an expert in the Information Technology Division of the National High-tech R&D program (863 Program), and a member of the Consultant Committee on International Cooperation of the National Natural Science Foundation of China. His research is in the broad area of wireless communications with emphasis on the joint source-channel coding solutions, novel coding design, and model-driven approaches for semantic communications.



**Marwan Krunz** (Fellow, IEEE) is a Regents Professor at the University of Arizona. He holds the Kenneth VonBehren Endowed Professorship in ECE and is also a professor of computer science. He directs the Broadband Wireless Access and Applications Center (BWAC), a multi-university NSF/industry center that focuses on next-generation wireless technologies. He also holds a courtesy appointment as a professor at the University Technology Sydney. Previously, he served as the site director for Connection One, an NSF/industry-funded center of five universities and 20+ industry affiliates. Dr. Krunz's research is in the fields of wireless communications, networking, and security, with recent focus on applying AI and machine learning techniques for protocol adaptation, resource management, and signal intelligence. He has published more than 320 journal articles and peer-reviewed conference papers, and is a named inventor on 12 patents. His latest h-index is 60. He is an IEEE Fellow, an Arizona Engineering Faculty Fellow, and an IEEE Communications Society Distinguished Lecturer (2013-2015). He received the NSF CAREER award. He served as the Editor-in-Chief for the IEEE Transactions on Mobile Computing. He also served as editor for numerous IEEE journals. He was the TPC chair for INFOCOM'04, SECON'05, WoWMoM'06, and Hot Interconnects 9. He was the general vice-chair for WiOpt 2016 and general co-chair for WiSec'12. Dr. Krunz served as chief scientist/technologist for two startup companies that focus on 5G and beyond wireless systems.

## APPENDIX A

### PROOFS OF THEOREM 1 AND COROLLARY 1

#### A.1 Auxiliary Lemmas

**Lemma 1.** Suppose Assumption 1 holds. Consider the sequence  $\{\Omega_{m,t}\}_{t=1}^T$  generated by static-weighting-based solution. Define

$$A_1 = \frac{1}{T} \mathbb{E} \left[ \sum_{i \in \{a,p,n\}} \gamma_{m,0}^i (\mathcal{L}_m^i(\Omega_{m,0}, \mathcal{D}^i) - \mathcal{L}_m^i(\Omega_{m,T}, \mathcal{D}^i)) \right],$$

$$A_2 = \frac{1}{T} \sum_{t=0}^{T-1} \mathbb{E} \left[ \left\| \sum_{i \in \{a,p,n\}} \gamma_{m,t}^i \nabla \ell_m^i(\Omega_{m,t}, d_t^i) \right\|^2 \right].$$

Then, it holds that

$$\frac{1}{T} \sum_{t=0}^{T-1} \mathbb{E} \left[ \left\| \sum_{i \in \{a,p,n\}} \gamma_m^i \nabla \mathcal{L}_m^i(\Omega_{m,t}, \mathcal{D}^i) \right\|^2 \right] \leq \frac{1}{\beta} A_1 + \frac{\beta \mu_g}{2} A_2.$$

*Proof.* We first establish that, for any given static weight  $\gamma_{m,0}^i$ , there exists an upper bound for the gap between the global losses in two consecutive coordination rounds. By leveraging the  $\mu_g$ -smoothness of  $\ell_m^i(\cdot)$ , we have

$$\begin{aligned} & \sum_{i \in \{a,p,n\}} \gamma_{m,0}^i (\mathcal{L}_m^i(\Omega_{m,t+1}, \mathcal{D}^i) - \mathcal{L}_m^i(\Omega_{m,t}, \mathcal{D}^i)) \\ & \leq \left\langle \sum_{i \in \{a,p,n\}} \gamma_{m,0}^i \nabla \mathcal{L}_m^i(\Omega_{m,t}, \mathcal{D}^i), \Omega_{m,t+1} - \Omega_{m,t} \right\rangle \\ & \quad + \frac{\mu_g}{2} \|\Omega_{m,t+1} - \Omega_{m,t}\|^2 \\ & = -\beta_t \left\langle \sum_{i \in \{a,p,n\}} \gamma_{m,0}^i \nabla \mathcal{L}_m^i(\Omega_{m,t}, \mathcal{D}^i), \sum_{i \in \{a,p,n\}} \gamma_{m,t}^i \nabla \ell_m^i(\Omega_{m,t}, d_t^i) \right\rangle \\ & \quad + \frac{\mu_g}{2} \beta_t^2 \left\| \sum_{i \in \{a,p,n\}} \gamma_{m,t}^i \nabla \ell_m^i(\Omega_{m,t}, d_t^i) \right\|^2. \end{aligned} \quad (18)$$

Note that for static-weighting scheme, the weight  $\gamma_{m,t}^i$  for each agent  $i$  remain constant across coordination rounds, i.e.,  $\gamma_{m,t}^i = \gamma_{m,0}^i$  for all  $t$ . Taking expectation over the random sample  $d_t^i$  on both sides of the above inequality, and setting the step size  $\beta_t = \beta \geq 0$ , we have

$$\begin{aligned} & \mathbb{E} \left[ \sum_{i \in \{a,p,n\}} \gamma_{m,0}^i (\mathcal{L}_m^i(\Omega_{m,t+1}, \mathcal{D}^i) - \mathcal{L}_m^i(\Omega_{m,t}, \mathcal{D}^i)) \right] \\ & \leq -\beta \mathbb{E} \left\| \sum_{i \in \{a,p,n\}} \gamma_{m,t}^i \nabla \mathcal{L}_m^i(\Omega_{m,t}, \mathcal{D}^i) \right\|^2 \\ & \quad + \frac{\mu_g}{2} \beta^2 \mathbb{E} \left\| \sum_{i \in \{a,p,n\}} \gamma_{m,t}^i \nabla \ell_m^i(\Omega_{m,t}, d_t^i) \right\|^2. \end{aligned} \quad (19)$$

Summing the the above inequality across all coordination rounds  $t = 0$  to  $T-1$  and rearranging terms, we obtain

$$\begin{aligned} & \frac{1}{T} \sum_{t=0}^{T-1} \mathbb{E} \left[ \left\| \sum_{i \in \{a,p,n\}} \gamma_m^i \nabla \mathcal{L}_m^i(\Omega_{m,t}, \mathcal{D}^i) \right\|^2 \right] \\ & \leq \frac{1}{\beta T} \mathbb{E} \left[ \sum_{i \in \{a,p,n\}} \gamma_m^i (\mathcal{L}_m^i(\Omega_{m,0}, \mathcal{D}^i) - \mathcal{L}_m^i(\Omega_{m,T}, \mathcal{D}^i)) \right] \\ & \quad + \frac{\beta \mu_g}{2} \mathbb{E} \left[ \left\| \sum_{i \in \{a,p,n\}} \gamma_m^i \nabla \ell_m^i(\Omega_{m,t}, d_t^i) \right\|^2 \right]. \end{aligned} \quad (20)$$

This concludes the proof.  $\square$

**Lemma 2 (Lemma 19 [38]).** Suppose Assumption 1 holds. Consider the sequence  $\{\Omega_{m,t}\}_{t=1}^T$  generated by dynamic-weighting scheme. Further define

$$A_3 =$$

$$\frac{1}{T} \sum_{t=0}^{T-1} \mathbb{E} \left[ \left\| \sum_{i \in \{a,p,n\}} \gamma_{m,t}^i \nabla \ell_m^i(\Omega_{m,t}, d_{t(1)}^i)^\top \nabla \ell_m^i(\Omega_{m,t}, d_{t(2)}^i) \right\|^2 \right],$$

$$A_4 =$$

$$\begin{aligned} & \frac{1}{T} \sum_{t=0}^{T-1} \mathbb{E} \left[ \left\| \sum_{i \in \{a,p,n\}} \gamma_{m,t}^i \nabla \ell_m^i(\Omega_{m,t}, d_{t(1)}^i)^\top \nabla \ell_m^i(\Omega_{m,t}, d_{t(2)}^i) \right\|^2 \right. \\ & \quad \left. \left\| \sum_{i \in \{a,p,n\}} \gamma_{m,0}^i \nabla \mathcal{L}_m^i(\Omega_{m,t}, \mathcal{D}^i)^\top \nabla \mathcal{L}_m^i(\Omega_{m,t}, \mathcal{D}^i) \right\|^2 \right], \end{aligned}$$

Then, it holds that

$$\begin{aligned} & \frac{1}{T} \sum_{t=0}^{T-1} \mathbb{E}_{\mathcal{A}} \left[ \left\| \sum_{i \in \{a,p,n\}} \gamma_{m,t}^i l_m^i(\Omega_{m,t}, \mathcal{D}^i) \right\|^2 \right] \\ & \leq \frac{1}{\beta} A_1 + \frac{\beta \mu_g}{2} A_2 + \frac{\eta}{2} A_3 + \eta A_4. \end{aligned} \quad (21)$$

#### A.2 Proof of Theorem 1

According to Lemma 1, under Assumption 1-3, we have

$$\begin{aligned} & \frac{1}{T} \sum_{t=0}^{T-1} \mathbb{E} \left[ \left\| \sum_{i \in \{a,p,n\}} \gamma_m^i \nabla \mathcal{L}_m^i(\Omega_{m,t}, \mathcal{D}^i) \right\|^2 \right] \\ & \leq \frac{1}{\beta} A_1 + \frac{\beta \mu_g}{2} A_2 \leq \frac{c_I}{\beta T} + \frac{\beta \mu_g \mu_l^2}{2}, \end{aligned} \quad (22)$$

where the last inequality follows from the Lipschitz continuity of  $\ell_m^i(\cdot)$  in Assumption 2, which ensures  $A_2 \leq \mu_l^2$ .

Then, by the Jensen's inequality and the convexity of the square function, as well as the sub-additivity of the square root function, it holds that

$$\begin{aligned} & \frac{1}{T} \sum_{t=0}^{T-1} \mathbb{E} \left[ \left\| \sum_{i \in \{a,p,n\}} \gamma_m^i \nabla \mathcal{L}_m^i(\Omega_{m,t}, \mathcal{D}^i) \right\| \right] \\ & \leq \left( \frac{1}{T} \sum_{t=0}^{T-1} \mathbb{E} \left[ \left\| \sum_{i \in \{a,p,n\}} \gamma_m^i \nabla \mathcal{L}_m^i(\Omega_{m,t}, \mathcal{D}^i) \right\|^2 \right] \right)^{\frac{1}{2}} \\ & \leq \sqrt{\frac{c_I}{\beta T}} + \sqrt{\frac{\beta \mu_g \mu_l^2}{2}} = \mathcal{O}(\beta^{-\frac{1}{2}} T^{-\frac{1}{2}} + \beta^{\frac{1}{2}}). \end{aligned} \quad (23)$$

This completes the proof.

#### A.3 Proof of Corollary 1

The proof follows a similar structure to that of Theorem 1. According to Lemma 2, under Assumption 1-3, it holds that

$$\begin{aligned} & \frac{1}{T} \sum_{t=0}^{T-1} \mathbb{E} \left[ \left\| \sum_{i \in \{a,p,n\}} \gamma_{m,t}^i \nabla \mathcal{L}_m^i(\Omega_{m,t}, \mathcal{D}^i) \right\|^2 \right] \\ & \leq \frac{1}{\beta} A_1 + \frac{\beta \mu_g}{2} A_2 + \frac{\eta}{2} A_3 + \eta A_4 \\ & \leq \frac{c_I}{\beta T} + \frac{9}{2} \eta \mu_l^4 + \frac{1}{2} \beta \mu_g \mu_l^2, \end{aligned} \quad (24)$$

where the last inequality comes from the fact that 1)  $A_3 \leq 3\mu_l^4$  and 2)  $A_4 \leq 3\mu_l^4$ , which results from the smoothness in Assumption 1.

Then, following the same reasoning as in the proof of Theorem 1, we apply Jensen's inequality and the subadditivity of the square root to derive:

$$\begin{aligned} & \frac{1}{T} \sum_{t=0}^{T-1} \mathbb{E} \left[ \left\| \sum_{i \in \{a, p, n\}} \gamma_{m,t}^i \nabla \mathcal{L}_m^i(\boldsymbol{\Omega}_{m,t}, \mathcal{D}^i) \right\| \right] \\ & \leq \left( \frac{1}{T} \sum_{t=0}^{T-1} \mathbb{E} \left[ \left\| \sum_{i \in \{a, p, n\}} \gamma_{m,t}^i \nabla \mathcal{L}_m^i(\boldsymbol{\Omega}_{m,t}, \mathcal{D}^i) \right\|^2 \right] \right)^{\frac{1}{2}} \\ & \leq \sqrt{\frac{c_I}{\beta T}} + 3 \sqrt{\frac{\eta \mu_l^4}{2}} + \sqrt{\frac{\beta \mu_g \mu_l^2}{2}} \\ & = \mathcal{O}(\beta^{-\frac{1}{2}} T^{-\frac{1}{2}} + \eta^{\frac{1}{2}} + \beta^{\frac{1}{2}}). \end{aligned} \quad (25)$$

This concludes the proof.

## APPENDIX B PROOFS OF THEOREM 2 AND COROLLARY 2

### B.1 Auxiliary Lemmas

**Lemma 3** (Theorem 16 [48]). Let  $\mathcal{D} = \bigcup_{i \in \{a, p, n\}} \mathcal{D}^i$  and  $\tilde{\mathcal{D}} = \bigcup_{i \in \{a, p, n\}} \tilde{\mathcal{D}}^i$  be two identical training datasets except that only the  $k$ th data sample  $d_k^j$  in dataset  $\mathcal{D}^j$  is different. Let  $\mathcal{I}_{\mathcal{D}^i}(\mathcal{A}_m) = \{s_{m,t}^i\}_{t=1}^T$  represent the random index sequence of samples in dataset  $\mathcal{D}^i$  to compute stochastic gradients during each training round. If for any data sample  $d^i \in \mathcal{D}^i$ ,

$$\sup_{d^i} \mathbb{E} \left[ \left\| \sum_{i \in \{a, p, n\}} \gamma_m^i \nabla \ell_m^i(\mathcal{A}_m(\mathcal{D}), d^i) \right\|^2 \mid k \in \mathcal{I}_{\mathcal{D}^j}(\mathcal{A}_m) \right] \leq G^2.$$

Then, we have

$$\begin{aligned} & \sup_{d^i} \mathbb{E} \left[ \left\| \sum_{i \in \{a, p, n\}} \gamma_m^i (\nabla \ell_m^i(\mathcal{A}_m(\mathcal{D}), d^i) - \nabla \ell_m^i(\mathcal{A}_m(\tilde{\mathcal{D}}), d^i)) \right\|^2 \right] \\ & \leq 4G^2 \cdot \mathbb{P}(k \in \mathcal{I}_{\mathcal{D}^j}(\mathcal{A}_m)). \end{aligned} \quad (26)$$

**Lemma 4** (Theorem 6 [48]). Suppose for any data sample  $d^i \in \mathcal{D}^i$ , the loss function  $\ell_m^i(\boldsymbol{\Omega}_m, d^i)$  is differentiable. If a randomized algorithm  $\mathcal{A}$  is uniformly stable with  $\epsilon$ , then

$$\begin{aligned} & \mathbb{E}_{\mathcal{A}, \mathcal{D}} \left[ \left\| \sum_{i \in \{a, p, n\}} \gamma_m^i (\nabla \ell_m^i(\mathcal{A}_m(\mathcal{D}), \mathcal{D}^i) - \nabla \tilde{\ell}_m^i(\mathcal{A}_m(\tilde{\mathcal{D}}), \mathcal{D}^i)) \right\|^2 \right] \\ & \leq 4\epsilon + \sqrt{\frac{V}{D}}, \end{aligned} \quad (27)$$

where

$$V = \mathbb{E} \left[ \left\| \sum_{i \in \{a, p, n\}} \gamma_m^i (\nabla \ell_m^i(\mathcal{A}_m(\mathcal{D}), d^i) - \mathbb{E}[\nabla \ell_m^i(\mathcal{A}_m(\mathcal{D}), d^i)]) \right\|^2 \right]$$

denotes the variance of gradients.

### B.2 Proof of Theorem 2

Based on Lemma 3, the uniform stability parameter in Definition 5 can be bounded by

$$\epsilon^2 \leq 4G^2 \cdot \mathbb{P}(k \in \mathcal{I}_{\mathcal{D}^j}(\mathcal{A}_m)). \quad (28)$$

Let  $s_t^i$  be the index of sample in dataset  $\mathcal{D}^i$  selected by algorithm  $\mathcal{A}$  at  $t$ th coordination,  $\mathcal{I}_{\mathcal{D}^i,t}(\mathcal{A}_m)$  be the indices of samples in dataset  $\mathcal{D}^i$  selected by algorithm  $\mathcal{A}$  up to the  $t$ -th iteration. Then,

$$\begin{aligned} \mathbb{P}(j \in \mathcal{I}_{\mathcal{D}^i,t}(\mathcal{A}_m)) &= \mathbb{P} \left( \bigcup_{\tau=1}^t \{s_\tau^i = j\} \right) \\ &\leq \sum_{\tau=1}^t \mathbb{P}\{s_\tau^i = j\} = \frac{t}{D}. \end{aligned} \quad (29)$$

Substituting (29) into (28), the uniform stability parameter of the  $t$ -th iteration is upper bounded by

$$\epsilon^2 \leq \frac{4G^2 t}{D} \leq \frac{4G^2 T}{D}. \quad (30)$$

Then, based on Lemma 4, the G-error is upper bounded by

$$\begin{aligned} \mathbb{E}_{\mathcal{A}, \mathcal{D}}[\mathcal{E}_G] &\leq 4\epsilon + \sqrt{\frac{V}{D}} \\ &\leq 8G \sqrt{\frac{T}{D}} + \sqrt{\frac{V}{D}} = \mathcal{O}(T^{\frac{1}{2}} D^{-\frac{1}{2}}). \end{aligned} \quad (31)$$

This concludes the proof.

### B.3 Proof of Corollary 2

The proof of Corollary 2 reveals that the algorithm's stochasticity originates solely from the random sampling process at each iteration. As the conflict-resolving mechanism preserves this sampling distribution, we conclude that the upper bound on the G-error remains unchanged. Refer to Appendix B.2 for a detailed proof.

## APPENDIX C PROOFS OF THEOREM 3 AND THEOREM 4

### C.1 Auxiliary Lemmas

**Lemma 5** (Lemma 18 [38]). Suppose Assumption 1 holds.

Consider the sequence  $\{\boldsymbol{\Omega}_{m,t}\}_{t=1}^T$  and  $\{\gamma_{m,t}\}_{t=1}^T$  generated by dynamic weighting algorithm with step size  $\beta_t = \beta \geq 0$ ,  $\eta_t = \eta \geq 0$ . Follow the definition of  $A_3$  in Lemma 2 and define

$$A_5 = \frac{1}{T} \sum_{t=0}^{T-1} \mathbb{E} \left[ \left\| \sum_{i \in \{a, p, n\}} [\nabla \mathcal{L}_m^i(\boldsymbol{\Omega}_{m,t}, \mathcal{D}^i) + \nabla \mathcal{L}_m^i(\boldsymbol{\Omega}_{m,t+1}, \mathcal{D}^i)] \right\| \right. \\ \left. + \left\| \sum_{i \in \{a, p, n\}} \gamma_{m,t+1}^i \nabla \ell_m^i(\boldsymbol{\Omega}_{m,t}, d^i) \right\| \right].$$

Then it holds that

$$\begin{aligned} & \frac{1}{T} \sum_{t=0}^{T-1} \mathbb{E} \left[ \left\| \sum_{i \in \{a, p, n\}} \gamma_{m,t}^i \nabla \mathcal{L}_m^i(\boldsymbol{\Omega}_m, \mathcal{D}^i) \right\|^2 \right. \\ & \quad \left. - \left\| \sum_{i \in \{a, p, n\}} \gamma_{m,t}^{i*} \nabla \mathcal{L}_m^i(\boldsymbol{\Omega}_m, \mathcal{D}^i) \right\|^2 \right] \\ & \leq \rho + \frac{4}{\eta T} (1 + \sqrt{3} \rho^{-1} \beta T \mu_g A_5) + \eta A_3, \end{aligned} \quad (32)$$

where  $\rho$  is a strictly positive parameter and is used for analysis but not for algorithm update such that

$$\begin{aligned} \gamma_{m,t}^* &= \langle \gamma_{m,t}^{a*}, \gamma_{m,t}^{p*}, \gamma_{m,t}^{n*} \rangle = \\ &= \arg \min_{\gamma} \frac{1}{2} \left\| \sum_{i \in \{a,p,n\}} \gamma_{m,t}^{i*} \nabla \mathcal{L}_m^i(\Omega_m, \mathcal{D}^i) \right\|^2 + \frac{\rho}{2} \|\gamma\|^2. \end{aligned} \quad (33)$$

## C.2 Proof of Theorem 3

We will present the upper and lower bounds of the conflict error under the static weighting algorithm, respectively. Let  $\mathcal{E}_C(\Omega_{m,t}, \gamma_{m,t})$  denote the conflict error associated with model parameters  $\Omega_{m,t}$  and weight vector  $\gamma_{m,t} = \langle \gamma_{m,t}^a, \gamma_{m,t}^p, \gamma_{m,t}^n \rangle$ .

First, for the upper bound, it holds that

$$\begin{aligned} &\mathcal{E}_C(\Omega_{m,T}, \gamma_{m,T}) \\ &= \mathbb{E} \left[ \left\| \sum_{i \in \{a,p,n\}} (\gamma_{m,T}^i - \gamma_{m,T}^{i*}) \nabla \mathcal{L}_m^i(\Omega_{m,T}, \mathcal{D}^i) \right\|^2 \right] \leq 4G^2, \end{aligned} \quad (34)$$

where the inequality comes from the Assumption 4.

Second, by defining  $\tilde{i} = \arg \min_{i \in \{a,p,n\}} \mathbb{E}[\gamma_{m,t}^{i*}(\Omega_{m,t})]$ , we can prove the lower bound as follows. By the pigeonhole principle, we can easily have  $\mathbb{E}[\gamma_{m,t}^{\tilde{i}}(\Omega_{m,t})] \leq \frac{1}{3}$  for any given  $t$ , then there exists  $\gamma_{m,T}^{\tilde{i}} = 1$  such that

$$\begin{aligned} &\mathcal{E}_C(\Omega_{m,T}, \gamma_{m,T}) \\ &= \mathbb{E} \left[ \left\| \sum_{i \in \{a,p,n\}} (\gamma_{m,T}^{\tilde{i}} - \gamma_{m,T}^{\tilde{i}*}) \nabla \mathcal{L}_m^i(\Omega_{m,T}, \mathcal{D}^i) \right\|^2 \right] \\ &\geq (1 - \frac{1}{3})^2 G^2 \geq \frac{4}{9} G^2. \end{aligned} \quad (35)$$

Combining the upper and lower bounds in (34) and (35) yields the result.

## C.3 Proof of Theorem 4

First, building on the result in Lemma 5, we have

$$\begin{aligned} &\frac{1}{T} \sum_{t=0}^{T-1} \mathbb{E} \left[ \left\| \sum_{i \in \{a,p,n\}} (\gamma_{m,t}^i - \gamma_{m,t}^{i*}) \nabla \mathcal{L}_m^i(\Omega_m, \mathcal{D}^i) \right\|^2 \right] \\ &\leq \frac{1}{T} \sum_{t=0}^{T-1} \mathbb{E} \left[ \left\| \sum_{i \in \{a,p,n\}} \gamma_{m,t}^i \nabla \mathcal{L}_m^i(\Omega_m, \mathcal{D}^i) \right\|^2 \right. \\ &\quad \left. - \left\| \sum_{i \in \{a,p,n\}} \gamma_{m,t}^{i*} \nabla \mathcal{L}_m^i(\Omega_m, \mathcal{D}^i) \right\|^2 \right] \\ &\leq \rho + \frac{4}{\eta T} (1 + \sqrt{3} \rho^{-1} \beta T \ell_f A_5) + \eta A_3, \end{aligned} \quad (36)$$

where the first inequality comes from the triangle inequality.

Next, we derive the C-error of  $t$ th coordination as follows

$$\begin{aligned} &\mathcal{E}_C(\Omega_{m,t}, \gamma_{m,t}) \\ &= \left\| \sum_{i \in \{a,p,n\}} (\gamma_{m,t}^i - \gamma_{m,t}^{i*}) \nabla \mathcal{L}_m^i(\Omega_{m,t}, \mathcal{D}^i) \right\|^2 \\ &= \left\| \sum_{i \in \{a,p,n\}} \gamma_{m,t}^i \nabla \mathcal{L}_m^i(\Omega_{m,t}, \mathcal{D}^i) \right\|^2 \\ &\quad + \left\| \sum_{i \in \{a,p,n\}} \gamma_{m,t}^{i*} \nabla \mathcal{L}_m^i(\Omega_{m,t}, \mathcal{D}^i) \right\|^2 \\ &\quad - 2 \left\langle \sum_{i \in \{a,p,n\}} \gamma_{m,t}^i \nabla \mathcal{L}_m^i(\Omega_{m,t}, \mathcal{D}^i), \sum_{i \in \{a,p,n\}} \gamma_{m,t}^{i*} \nabla \mathcal{L}_m^i(\Omega_{m,t}, \mathcal{D}^i) \right\rangle \\ &\leq \left\| \sum_{i \in \{a,p,n\}} \gamma_{m,t}^i \nabla \mathcal{L}_m^i(\Omega_{m,t}, \mathcal{D}^i) \right\|^2 \\ &\quad - \left\| \sum_{i \in \{a,p,n\}} \gamma_{m,t}^{i*} \nabla \mathcal{L}_m^i(\Omega_{m,t}, \mathcal{D}^i) \right\|^2, \end{aligned}$$

where the inequality comes from the fact that

$$\left\| \sum_{i \in \{a,p,n\}} \gamma_{m,t}^i \nabla \mathcal{L}_m^i(\Omega_{m,t}, \mathcal{D}^i) \right\|^2 \geq \left\| \sum_{i \in \{a,p,n\}} \gamma_{m,t}^{i*} \nabla \mathcal{L}_m^i(\Omega_{m,t}, \mathcal{D}^i) \right\|^2.$$

By averaging the results of each coordination and choosing  $\rho = 2(3\beta\mu_g\mu_l^2/\eta)^{\frac{1}{2}}$ , we have

$$\begin{aligned} &\frac{1}{T} \sum_{t=0}^{T-1} \mathbb{E}[\mathcal{E}_C(\Omega_{m,t}, \gamma_{m,t})] \\ &\leq \frac{1}{T} \sum_{t=0}^{T-1} \mathbb{E} \left[ \left\| \sum_{i \in \{a,p,n\}} (\gamma_{m,t}^i - \gamma_{m,t}^{i*}) \nabla \mathcal{L}_m^i(\Omega_{m,t}, \mathcal{D}^i) \right\|^2 \right] \\ &\leq \rho + \frac{4}{\eta T} (1 + 6\rho^{-1} \beta T \mu_g \mu_l^2) + \eta \cdot 3\mu_l^4 \\ &= \frac{4}{\eta T} + 6 \sqrt{3\mu_g \mu_l^2 \frac{\beta}{\eta}} + 3\eta \mu_l^4, \end{aligned} \quad (37)$$

where the last inequality comes from that  $A_3 \leq 3\mu_l^4$  and  $A_5 \leq 2\sqrt{3}\mu_l^2$ . This completes the proof.